PHILOSOPHICAL TRANSACTIONS OF THE ROYAL SOCIETY A MATHEMATICAL, PHYSICAL & ENGINEERING SCIENCES

Critical Lines and Phase Equilibria in Binary Van Der Waals Mixtures

P. H. Van Konynenburg and R. L. Scott

Phil. Trans. R. Soc. Lond. A 1980 **298**, 495-540
doi: 10.1098/rsta.1980.0266

CRITICAL LINES AND PHASE EQUILIBRIA IN BINARY VAN DER WAALS MIXTURES

By P. H. VAN KONYNENBURG† and R. L. SCOTT
Department of Chemistry, University of California, Los Angeles, California 90024, *U.S.A.*

(*Communicated by J. S. Rowlinson, F.R.S. – Received* 12 *June* 1979)

CONTENTS

The van der Waals equation of state is used to determine phase diagrams for a wide variety of binary fluid mixtures. The locus of the critical line in pressure–temperature-composition space is determined exactly by solving a set of equations with the aid of a computer.

The van der Waals constants a_m and b_m for the mixture depend quadratically and linearly upon the mole fractions x_i: $a_m = \Sigma_i \Sigma_j x_i x_j a_{ij}$ and $b_m = \Sigma_i x_i b_{ii}$. Mixtures are characterized by three non-dimensional parameters: $\xi = (b_{22} - b_{11})/(b_{11} + b_{22})$, $\zeta = (a_{22} b_{22}^{-2} - a_{11} b_{11}^{-2})/(a_{11} b_{11}^{-2} + a_{22} b_{22}^{-2})$ and $\Lambda = (a_{11} b_{11}^{-2} - 2a_{12}/b_{11} b_{22} + a_{22} b_{22}^{-2})/(a_{11} b_{11}^{-2} + a_{22} b_{22}^{-2})$. The parameter Λ can be related to the low-temperature enthalpy of mixing and the parameter ζ to the difference between the gas–liquid critical pressures of the pure fluids.

Most of the calculations are for molecules of equal size ($\xi = 0$), but calculations for a size ratio of two ($\xi = \frac{1}{3}$) are also reported. Nine characteristic types of critical lines are distinguished and these correspond to nine separate regions on a Λ, ζ-diagram. Isobaric temperature-composition diagrams and pressure–temperature projections are given for one example from each region to illustrate the possible types of phase equilibrium.

Special attention is given to the details of lower critical solution temperature behaviour (type IV) such as is found in the system methane + *n*-hexane, to tricritical

† Present address: Raychem Corporation, Menlo Park, California 94025, U.S.A.

points (symmetrical and unsymmetrical), to azeotropy, and to the possibility of double azeotropy.

The phase diagrams calculated from the van der Waals equation seem to account, at least qualitatively, for all but one of the varieties of phase equilibria found in binary fluid mixtures: the low-temperature lower critical solution points in some highly structured aqueous solutions of alcohols and amines.

[*Introductory note.* This article reproduces, largely unchanged, a major portion of the U.C.L.A. Ph.D. dissertation of P. H. van Konynenburg (1968). Except for short extracts reported in other papers (Scott & van Konynenburg 1970; Scott 1971), little of this detailed material has yet been published. However, more than fifty copies of the dissertation were distributed and there have been repeated references to the work in other articles and books (for example, Hicks & Young 1975; Furman *et al.* 1977; Clancy *et al.* 1978), and the examples and classifications are well, if not widely, known. The work reported here has continued at U.C.L.A. and has been extended to other equations of state, and subsequent papers will need the detailed background originally presented. After ten years, however, the subject has progressed and a failure to mention any subsequent work, here and elsewhere, would be unfair to all concerned. On the other hand, to present a completely revised paper would misrepresent the extent of our understanding in 1968. The text that follows derives primarily from chapters II and III of the dissertation that are reproduced, essentially verbatim, except for some minor editorial changes and a change of symbols (ζ, Λ, etc.) to conform to the usage in our 1970 paper. Substantive comments and second thoughts that postdate the 1968 dissertation are always enclosed in square brackets.]

1. Introduction

The study of phase equilibria is historically one of the most important sources of information about the nature of intermolecular forces in non-electrolyte liquids and their mixtures. Many of the main features of vapour–liquid and liquid–liquid phase behaviour were already well characterized experimentally during the early part of this century, but the theoretical explanation of phase equilibria for a wide variety of substances and over a large range of pressures and temperatures has lagged far behind. This paper presents theoretical studies of phase equilibria in binary mixtures obeying the van der Waals equation, especially liquid–liquid equilibria that can occur at high pressures.

The variety of fluid phase behaviour that occurs in binary mixtures can be qualitatively discussed in terms of the changes in thermodynamic properties near critical points.

Upper critical solution temperatures (UCSTs) occur when a heterogeneous (two-phase) system becomes a homogeneous (one-phase) system when the temperature is raised. The maximum temperature along the temperature–mole fraction (T, x) coexistence curve for constant pressure is the UCST at this pressure. Lower critical solution temperatures (LCSTs) occur when a homogeneous system becomes a two-phase system when the temperature is increased. The LCST is at the minimum of the T, x coexistence curve. Thermodynamic considerations of critical points yield requirements for the curvature of the mixing functions plotted against x. At any critical point,

$$\left(\frac{\partial^2 G_m}{\partial x^2}\right)_{T,p} = 0, \quad \left(\frac{\partial^3 G_m}{\partial x^3}\right)_{T,p} = 0, \tag{1}$$

where G_m is the molar Gibbs free energy of the binary mixture.

UCSTs are present in most systems that have large positive molar excess enthalpies H_m^E. In practice, systems with small positive values of H_m^E or high melting temperatures may have metastable UCSTs that lie below a solid boundary [Dickinson *et al.* 1973]. LCSTs can occur in systems with negative excess enthalpy if the excess entropy is sufficiently negative to make the excess Gibbs free energy large and positive.

The phase behaviour of a one-component system can be described by any two of the variables temperature, T, pressure, p, and molar volume, V_m. For example, a p,T-phase diagram can be divided into regions where the liquid or gas phases are stable, separated by two-phase lines. The liquid–gas phase boundary (the vapour-pressure curve) ends at a gas–liquid critical *point*; beyond this point there is no liquid–gas equilibrium. Unlike the vapour-pressure curve, the solid–liquid boundary has no critical point.

To describe the phase behaviour of a binary mixture at least three of the variables T, p, V_m, and x must be used, the most convenient being T, p, and x. On a p,T-plane each pure component (designated 1 and 2 in order of increasing gas–liquid critical temperature) of a mixture is represented by its vapour-pressure curve. Mixing of the two components adds a third dimension: composition (expressed as the mole fraction x of component 2). The locus of the critical points of a mixture (i.e. the points where two phases become identical in density and composition) is represented by a critical *line* in p,T,x-space. In this paper only the projection of the critical lines on the p,T-plane will be shown in two-dimensional figures.

Experimental binary-fluid phase diagrams can be classified into three main groups:

Class 1. Mixtures of two components with similar gas–liquid critical temperatures. In such mixtures the critical points of the pure components are continuously connected by a critical line.

Class 2. Mixtures of two components with very different gas–liquid critical temperatures. In these mixtures there is no continuous critical line joining the critical points of the pure components.

Class 3. Very complex mixtures exhibiting such phenomena as low-temperature LCSTs. In this class the low-temperature phase behaviour results from strong specific interactions between the two components. These interactions lead to a high degree of order in the liquid mixture and thus cannot be represented by a 'one-fluid' equation of state such as that of van der Waals.

Many examples of experimental binary-fluid phase diagrams have been discussed by Rowlinson (1959, 1969) and by Schneider (1966).

Of the many alternative theoretical approaches that attempt to explain the thermodynamic properties of liquid mixtures, the earliest was that of van der Waals (1890). He applied the empirical concept of corresponding states to mixtures by assuming that a mixture behaves like a single fluid and, in particular, tied all prediction and discussion to his equation of state. This approach played an important role in the early interpretation of phase diagrams and critical lines in mixtures (van der Waals 1899, 1900, 1906–12; Kamerlingh Onnes *et al.* 1900–1907; van Laar 1904–1910).

The results of the early workers showed that, although the van der Waals equation gives only a qualitative description of the thermodynamic properties of liquid mixtures, it very rarely yields physically absurd results. Because the equations for the calculation of critical lines are difficult to solve, much of the early work was often sketchy and sometimes inaccurate, and remained incomplete. With the availability of fast modern computers and renewed theoretical interest in the 'classical' theory of dense fluids, the subject is being revived.

McKinnon (1967) made extensive calculations using this equation to predict vapour–liquid diagrams and gas–liquid critical points at high pressures and excess functions at zero pressure. His comparisons with experiment confirm that the van der Waals equation cannot provide a good quantitative interpretation of the properties of mixtures. [See also Marsh *et al.* (1970).] However we shall show here that most experimentally observed types of phase phenomena in binary mixtures (classes 1 and 2) can be produced from this equation of state. None of the systems cited as examples is expected to obey the van der Waals equation in detail; only the general (schematic) features of its phase equilibria can be predicted.

2. The basic equations

The van der Waals equation of state is

$$p = \frac{RT}{V_m - b} - \frac{a}{V_m^2}, \tag{2}$$

where R is the molar gas constant. The parameter a is a measure of the attractive forces between the molecules and the parameter b is a measure of the size (intrinsic volume) of the molecules. If the conditions for the gas–liquid critical point in a one-component system,

$$(\partial p/\partial V_m)_T = 0, \quad (\partial^2 p/\partial V_m^2)_T = 0, \tag{3}$$

are applied to (2), the critical temperature, pressure and molar volume are obtained as functions of a and b:

$$T^c = \tfrac{8}{27}a/Rb, \quad p^c = \tfrac{1}{27}a/b^2, \quad V_m^c = 3b. \tag{4}$$

For a binary mixture of components 1 and 2, van der Waals replaced a and b by

$$a(x) = (1-x)^2 a_{11} + 2(1-x)x a_{12} + x^2 a_{22}, \tag{5}$$

$$b(x) = (1-x)^2 b_{11} + 2(1-x)x b_{12} + x^2 b_{22}, \tag{6}$$

where x is the mole fraction of component 2. The constants a_{11} and a_{22} are measures of the attractive forces between pairs of molecules of the pure components 1 and 2, respectively, and a_{12} is the corresponding parameter for the interaction between molecules 1 and 2. The constants b_{11}, b_{22} and b_{12} are size parameters (proportional to volume) for the pure components and for the mixed pairs. Equations (5) and (6) imply random mixing of the two components. [These 'one-fluid' equations do not conform to the strict statistical mechanical definition of 'random mixing', in which, for a given x, the radial distribution function $g_{\alpha\beta}(r)$ must be the same for all pairs. This point has been discussed by Rowlinson (1970) and by Scott (1970).]

If b_{12} is chosen as the arithmetic mean of b_{11} and b_{22} (as did van der Waals), i.e.

$$b_{12} = \tfrac{1}{2}(b_{11} + b_{22}),$$

then

$$b(x) = (1-x)\, b_{11} + x b_{22}. \tag{7}$$

A theoretically sounder approximation for b_{12} [for spherical molecules] is the Lorentz expression, $b_{12} = [\tfrac{1}{2}(b_{11}^{\frac{1}{3}} + b_{22}^{\frac{1}{3}})]^3$, but (7) must lead to qualitatively similar conclusions and for simplicity it has been used for all of the calculations. [Since the parts of the dissertation presented in detail in this paper are restricted to mixtures of molecules of the same size, the distinction between these two approximations disappears: $b_{12} = b_{11} = b_{22}$.]

A liquid is almost unexpanded ($V_m \approx b$) at very low temperatures or at very high pressures. If $V_{1,m} \approx b_{11}$, $V_{2,m} \approx b_{22}$ and $V_m \approx b$, then, by using (7), it follows that $V_m^E \approx 0$. In practice, systems are usually studied at low (reduced) temperatures, not at extremely high pressures. For this reason the molar heat of mixing (excess enthalpy) in the unexpanded state ($V_m \approx b$) is denoted by $H_m^E(T = 0)$ and can be shown to be

$$H_m^E(T = 0) = \left(\frac{a_{11}}{b_{11}^2} - \frac{2a_{12}}{b_{11}b_{22}} + \frac{a_{22}}{b_{22}^2}\right) \frac{x(1-x)\, b_{11}b_{22}}{(1-x)\, b_{11} + xb_{22}}. \tag{8}$$

If a_{12} is replaced by the geometric mean of a_{11} and a_{22}, then this expression is the same as one used by van Laar (1910) and is closely related to those derived later by Scatchard (1931) and by Hildebrand & Wood (1933).

It is convenient to describe the mixtures with three new parameters, ξ, ζ, and Λ, which are defined by

$$\xi = (b_{22} - b_{11})/(b_{11} + b_{22}), \tag{9}$$

$$\zeta = \left(\frac{a_{22}}{b_{22}^2} - \frac{a_{11}}{b_{11}^2}\right) \Big/ \left(\frac{a_{11}}{b_{11}^2} + \frac{a_{22}}{b_{22}^2}\right), \tag{10}$$

$$\Lambda = \left(\frac{a_{11}}{b_{11}^2} - \frac{2a_{12}}{b_{11}b_{22}} + \frac{a_{22}}{b_{22}^2}\right) \Big/ \left(\frac{a_{11}}{b_{11}^2} + \frac{a_{22}}{b_{22}^2}\right). \tag{11}$$

[These are the definitions that we introduced later (Scott & van Konynenburg 1970). The original parameters, $\eta = (a_{22} - a_{11})/(a_{11} + a_{22})$ and $\Delta = (a_{11} - 2a_{12} + a_{22})/(a_{11} + a_{22})$, proved inconvenient when $b_{11} \neq b_{22}$. For $b_{11} = b_{22}$ ($\xi = 0$), of course, $\eta = \zeta$ and $\Delta = \Lambda$.] For $b_{11} = b_{22}$, ζ and Λ are related to the difference in critical temperatures or pressures of the pure components and to $H_m^E(T = 0)$, respectively, as seen in (4) and (8).

For equal-size molecules in the limit $p = \infty$, $V_m = b$, the close-packed system has ideal entropy of mixing ($S_m^E = 0$) and the excess free energy becomes

$$G_m^E = H_m^E - TS_m^E = H_m^E(T = 0),$$

which, by using (8), can be written as

$$G_m^E = x(1-x)(a_{11} + a_{22} - 2a_{12})/b. \tag{12}$$

Guggenheim (1952) has called systems obeying (12) 'simple mixtures'.

If the conditions for a critical point

$$\left(\frac{\partial^2 G_m^E}{\partial x^2}\right)_{T,p} = -\frac{RT}{x(1-x)}$$

$$\left(\frac{\partial^3 G_m^E}{\partial x^3}\right)_{T,p} = -\frac{RT(1-2x)}{x^2(1-x)}$$

are applied to (12) it is found that

$$\left.\begin{aligned} x^c &= \tfrac{1}{2} \\ (G_m^E)^c &= \tfrac{1}{2}RT^c = \tfrac{1}{4}(a_{11} - 2a_{12} + a_{22})/b. \end{aligned}\right\} \tag{13}$$

For convenience this critical temperature is written in a reduced form, $T_m^\infty = T^c/T_1^c$ (where T_1^c, the gas–liquid critical temperature of component 1, is $\frac{8}{27}a_{11}/Rb$). In terms of ζ and Λ this becomes (for $\xi = 0$)

$$T_m^\infty = \tfrac{27}{8}\Lambda/(1-\zeta). \tag{14}$$

This critical point at infinite pressure, $C_m(T_m^\infty, \infty, \frac{1}{2})$, will be used to describe the course of some critical lines in subsequent sections.

For the molar Helmholtz free energy of a binary van der Waals mixture, using as a reference state (superscript $^\ominus$) the state of the ideal unmixed gases at a molar volume $V_m^\ominus$, one obtains

$$A_m(T, V_m) - A_m^\ominus(T, V_m^\ominus) = -a/V_m - RT \ln [(V_m - b)/V_m^\ominus] + RT[(1-x) \ln (1-x) + x \ln x]. \quad (15)$$

The conditions for a critical point in a binary mixture are most compactly expressed in terms of the Gibbs free energy of the mixture (1). However, since it is not convenient to calculate the Gibbs free energy by using the van der Waals equation, these equations are transformed into the equivalent equations for the Helmholtz free energy:

$$A_{2V} A_{2x} - A_{Vx}^2 = 0, \quad (16)$$

$$A_{3V} A_{2x}^2 - 3A_{2Vx} A_{Vx} A_{2x} + 3A_{V2x} A_{Vx}^2 - A_{3x} A_{2V} A_{Vx} = 0, \quad (17a)$$

$$A_{3x} A_{2V}^2 - 3A_{2Vx} A_{Vx} A_{2V} + 3A_{x2V} A_{Vx}^2 - A_{3V} A_{2x} A_{Vx} = 0, \quad (17b)$$

where the abbreviated notation used for multiple differentiation is that of Rowlinson (1959, 1969), $A_{nxmV} = (\partial^{n+m} A_m / \partial^n x \, \partial^m V_m)_T$.

Only two of these three equations are independent. By tedious but straightforward algebra it is possible to eliminate the temperature and obtain an equation for the critical line in terms of V_m and x. For convenience the final equations are written in terms of reduced variables, the main ones being $T_r = T/T_1^c$, $p_r = p/p_1^c$, $V_r = V_m/b$. (Note that the reduced volume defined here is *not* the conventional van der Waals reduced volume $V_{r,1}/V_m^c = \frac{1}{3}V_m/b$.)

Most of the calculations were done for $b_{11} = b_{22}$ ($\xi = 0$), for which the equation for the critical line (given in Appendix A) is seventh order in both V_r and x. For the general case ($b_{11} \neq b_{22}$) the corresponding equation is eighth order in V_r and fifteenth order in x.

For a chosen value of x the roots of the final equation appear to lie between $V_m/b = 1$ and $V_m/b = 3$ (that is, between the close-packed volume and the volume corresponding to the critical point in a one-component system). Each root calculated was used to compute the reduced temperature and pressure of the critical point of the mixture.

In the mathematical formulation there is essentially no difference between gas–liquid and liquid–liquid critical points for mixtures; both are points of incipient instability and the characteristic densities of the phases involved do not change the thermodynamic description. Since the van der Waals equation is continuous through metastable and unstable states, all gas–liquid and liquid–liquid critical points, whether on stable, metastable, or unstable portions of a critical line, are calculated by our procedure. The stable part of a critical line may end at an upper or lower critical end point where the critical line intersects a three-phase line. To determine such points and other details of the T, p, x-phase diagram it becomes necessary to use all the conditions applicable to two conjugate phases α and β in equilibrium:

$$T^\alpha = T^\beta, \quad p^\alpha = p^\beta, \quad \mu_1^\alpha = \mu_1^\beta, \quad \mu_2^\alpha = \mu_2^\beta, \quad (18)$$

where μ_1 and μ_2 are the chemical potentials of the two components. Our procedure was to plot, for fixed T and p, the logarithms of the activities λ_1 and λ_2 against each other and determine the point of intersection. Details are given in Appendix A.

3. Azeotropy

The van der Waals equation predicts that azeotropy occurs for a fixed value of ζ when Λ is sufficiently positive or negative. First a general equation for the azeotropic line will be derived and then the special features for $b_{11} = b_{22}$ ($\xi = 0$) will be discussed.

For two phases α and β (here, liquid and vapour) to be in equilibrium at an azeotropic point, one adds to the usual conditions for phase equilibrium (18) the additional condition $x^\alpha = x^\beta$. Since $G_m = (1-x)\mu_1 + x\mu_2$ and $\mu_1 = G_m - x(\partial G_m/\partial x)_{T,p}$ and $\mu_2 = G_m + (1-x)(\partial G_m/\partial x)_{T,p}$, it follows that if $x^\alpha = x^\beta$, $G_m^\alpha = G_m^\beta$ and $(\partial G_m^\alpha/\partial x)_{T,p} = (\partial G_m^\beta/\partial x)_{T,p}$. As mentioned before, it is easier to use the van der Waals equation with the Helmholtz free energy than with the Gibbs free energy. Since, quite generally, $(\partial G_m/\partial x)_{T,p} = (\partial A_m/\partial x)_{T,V_m}$, it follows that at an azeotropic point

$$(\partial A_m^\alpha/\partial x)_{T,V_m^\alpha} = (\partial A_m^\beta/\partial x)_{T,V_m^\beta}, \tag{19}$$

When combined with (15) this expression yields

$$\frac{RTb'}{V_m^\alpha - b} - \frac{a'}{V_m^\alpha} = \frac{RTb'}{V_m^\beta - b} - \frac{a'}{V_m^\beta},$$

where $a' = \mathrm{d}a/\mathrm{d}x$ and $b' = \mathrm{d}b/\mathrm{d}x$. The requirement of equal pressures ($p^\alpha = p^\beta$) permits the use of (2) to eliminate $RT/(V_m - b)$, which reduces the foregoing to a general equation for the azeotropic curve:

$$\left.\begin{aligned} \left(\frac{1}{V_m^\alpha/b_m} + \frac{1}{V_m^\beta/b_m}\right)\left[\frac{\mathrm{d}(\ln b)}{\mathrm{d}x}\right] - \frac{\mathrm{d}(\ln a)}{\mathrm{d}x} &= 0, \\ \text{or} \qquad \left(\frac{1}{V_m^\alpha/b_m} + \frac{1}{V_m^\beta/b_m}\right)\left(\frac{-2\xi}{1-w\xi}\right) + \frac{2(\zeta - w\Lambda)}{1-w\zeta-2z\Lambda} &= 0, \end{aligned}\right\} \tag{20}$$

where $w = 1-2x$ and $z = x(1-x) = \frac{1}{4}(1-w^2)$.

(a) *The special case* $\xi = 0$

When $b_{11} = b_{22}$, $\mathrm{d}b/\mathrm{d}x = 0$ and thus $\mathrm{d}a/\mathrm{d}x$ must vanish or, setting $\xi = 0$ in (20), $\zeta - w\Lambda = 0$. This is equivalent to writing for the composition x^{AZ} of the azeotrope

$$x^{AZ} = \frac{a_{11} - a_{12}}{a_{11} + a_{22} - 2a_{12}} = \frac{\Lambda - \zeta}{2\Lambda}. \tag{21}$$

The azeotropic behaviour is seen to appear at $x = 0$ when $a_{12} = a_{11}$, and at $x = 1$ when $a_{12} = a_{22}$. From the diagrams in subsequent sections it will be clear that these conditions can be interpreted (for $a_{22}/a_{11} > 1$) as the onset of positive and negative azeotropy, respectively.

Since the azeotropic composition is independent of temperature and pressure, the azeotropic curve on a p_r, T_r phase diagram scales directly with the vapour-pressure curves of the pure components. These curves end at a gas–liquid critical line at $p_r = T_r = a(x^{AZ})/a_{11} = (2\Lambda - \zeta^2 - \Lambda^2)/2\Lambda(1-\zeta)$. Calculations show that a cusp appears in the gas–liquid critical line at this point, a curiosity that is an artefact of the case $\xi = 0$. Experimental diagrams show that azeotropic lines meet critical lines tangentially (see, for example, Rowlinson (1959, 1969)), a feature confirmed by all our calculations where $\xi \neq 0$.

4. Phase diagrams for binary mixtures of equal-sized molecules

The possible phase diagrams predicted for van der Waals mixtures according to the procedures outlined in the previous section and in Appendix A are classified according to the nature of their p,T-projections. Mixtures in which the gas–liquid critical points of the pure components, $C_1(T_1, p_1, x = 0)$ and $C_2(T_2, p_2, x = 1)$, are connected by a continuous critical line belong to class 1; mixtures in which there is no continuous critical line connecting C_1 and C_2 belong to class 2. (Here and subsequently we use the notation T_1, p_1, T_2, p_2 and T_m^∞ for the *reduced* properties at C_1, C_2 and C_m, i.e. $T_1 = T_1^c/T_1^c = 1$, $p_2 = p_2^c/p_1^c$, etc.

The phase diagrams are further distinguished by the presence or absence of three-phase lines (L_1L_2G) and azeotrope lines (positive and negative) and by the way in which critical lines meet these. Critical lines may end in various ways. They end at the one-component gas–liquid critical points C_1 and C_2 and at the limiting upper critical solution point $C_m(T_m^\infty, \infty, x = \frac{1}{2})$ of a close-packed ($V_m = b$) 'liquid–liquid' system. In addition, critical lines may terminate at the ends of three-phase lines, at upper or lower critical endpoints (UCEPs or LCEPs). Azeotrope lines, if present, end at high pressures on critical lines (tangentially in real systems, at mathematical cusps in the critical line for the special case $b_{11} = b_{22}$).

The nine types of phase diagrams (for molecules of equal size, i.e. $b_{11} = b_{22}$ or $\xi = 0$) are represented by the regions on the Λ–ξ grid shown in figure 1. The types are as follows.

Class 1

I. One critical line: C_1 to C_2 (G–L).
I-A. The same as I, with the addition of a negative azeotrope.
II. Two critical lines: C_1 to C_2 (G–L); C_m to UCEP (L–L).
II-A. The same as II, with the addition of a positive azeotrope.

Class 2

III-HA. Two critical lines: C_1 to UCEP (G–L); C_m to C_2 (L–L to G–L). A three-phase line runs from a UCEP to $p = 0$, $T = 0$ at lower temperatures than the one-component vapour pressure curves, producing 'heteroazeotrope' behaviour.
III. The same as III-HA except that the three-phase line lies between the two one-component vapour-pressure curves.
IV. Three critical lines: C_1 to UCEP (G–L); LCEP to C_2 (L–L to G–L); C_m to UCEP (L–L).
V. Two critical lines: C_1 to UCEP (G–L); LCEP to C_2 (L–L to G–L).
V-A. The same as V, with the addition of a negative azeotrope.

In addition there are two subregions, III_m and $III\text{-}HA_m$ that differ from II Iand III-HA only in that there are minimum and maximum pressures in the critical line going from C_m to C_2. Therefore at certain fixed pressures there will be three critical temperatures, two UCSTs and one LCST.

Two combining rules that relate a_{12} to a_{11} and a_{22} are represented by lines on figure 1: The geometric mean (g.m.), which is frequently used in theories of mixtures for which

$$a_{12} = (a_{11}a_{22})^{\frac{1}{2}}, \tag{22}$$

is a circular curve $[(1-\Lambda)^2 = (1-\zeta)(1+\zeta)]$ with centre at $\Lambda = 1$, $\zeta = 0$ (—·—). The arithmetic-mean line (a.m.) is the abscissa ($\Lambda = 0$), where $a_{12} = \frac{1}{2}(a_{11}+a_{22})$.

Full lines on figure 1 are boundaries separating regions having characteristic p_r, T_r, x-phase diagrams. When a dashed boundary is crossed, only minor features of the phase diagrams change. The dotted curve is a mathematical double-point curve and represents the locus of points where two critical lines meet and exchange branches. This intersection is never in a stable region of the phase diagram and is thus of no physical importance; for this reason it will not be considered further here. When the dashed line labelled $T_m^\infty = T_2$ is crossed,

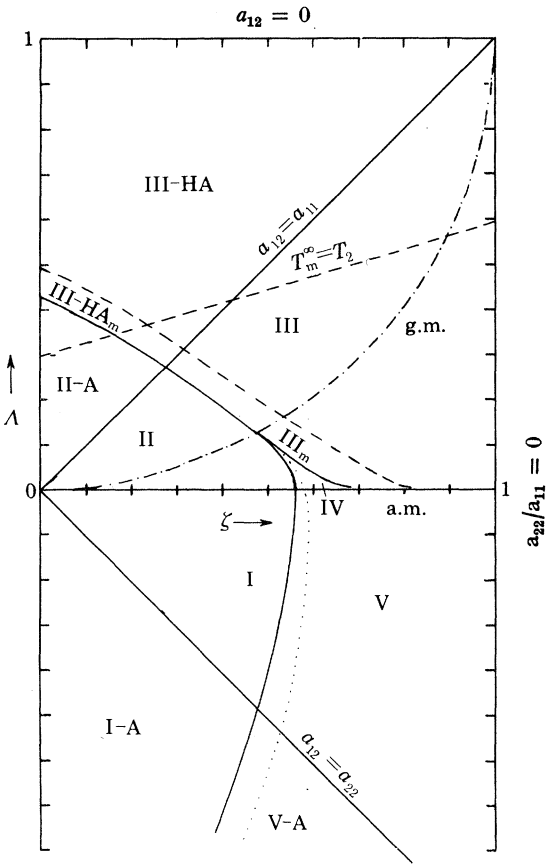

FIGURE 1. Diagram of phase behaviour for equal size molecules. Nine major regions of characteristic p,T-phase diagrams are separated by the boundaries (——). [The figure is incomplete in the region $\zeta = -0.08$ to 0.08, $\Lambda = 0{,}35$ to 0.48; this 'shield region' is shown in figure 38.]

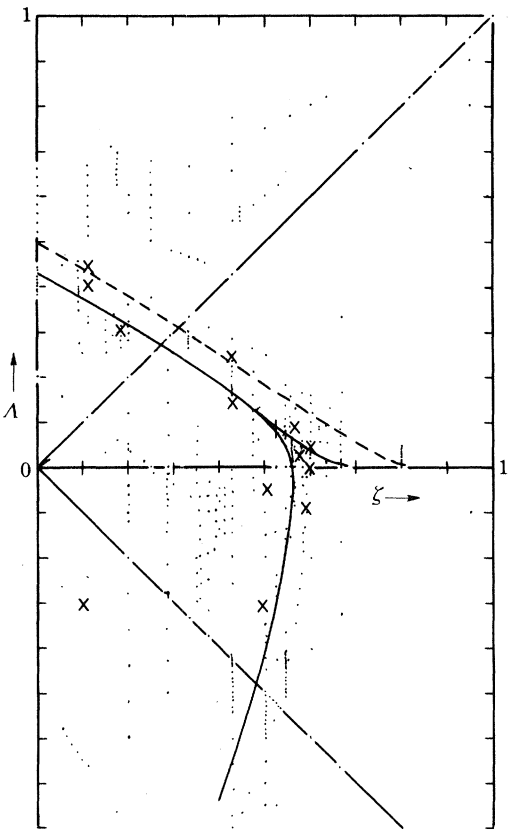

FIGURE 2. Values of ζ and Λ for which critical lines have been calculated to locate the main region boundaries and construct phase diagrams. Phase diagrams or p,T-projections for the systems × are shown in subsequent figures.

with increasing Λ, T_m^∞ becomes greater than T_2 (and, for $\zeta > 0$, greater than T_1 as well). [When fluid–fluid phase separation occurs at temperatures higher than the gas–liquid critical point of either pure component, the phenomenon is known as 'gas–gas immiscibility'. More than forty such binary systems have now been found; Schneider (1970) has contributed an authoritative review. For fits of simple equations of state to such phenomena see McGlashan *et al.* (1973, 1977) and Scott (1973).]

PHILOSOPHICAL TRANSACTIONS OF THE ROYAL SOCIETY A MATHEMATICAL, PHYSICAL & ENGINEERING SCIENCES

The diagram in figure 1 is closed at the top at the limit $a_{12} = 0$, where there are no 1–2 attractive forces, but there is no obvious physical limit at the bottom of the diagram for strong attractive forces. However the part shown probably includes all physically reasonable negative values of Λ. (The curved full-line boundary separating regions I-A and V-A and the dotted double-point curve intersect the Λ-axis ($\xi = 0$) at $\Lambda = -2.120$ and -2.806, respectively.) The dashed curved boundary between III_m and III and the full-line boundary between IV and III_m approach the ζ-axis asymptotically. [This last statement is now known to be incorrect. The IV–III_m boundary ends at $\zeta = \sqrt{2}/2 = 0.7071$, $\Lambda = 0$ and the III_m–III boundary ends at $\zeta = 3\sqrt{2}/5 = 0.8485$, $\Lambda = 0$.] The whole diagram is symmetrical with respect to reflexion about the Λ-axis. This mirror image results by interchanging the roles of a_{22} and a_{11}. Only the case $\zeta > 0$ is shown.

[This 'master diagram' (figure 1) is incomplete for a small area in the region $\Lambda = 0.35$ to 0.48, $\zeta = -0.08$ to 0.08, where there are phase diagrams of even greater complexity. We found some of this complexity when we calculated critical lines and phase diagrams for systems with $\zeta = 0$, but the full nature of this 'shield' region was first outlined by Furman *et al.* (1977) for a symmetrical model and then modified for a van der Waals binary mixture by Furman & Griffiths (1978). Further comments on the 'shield' region will be found in section (4*b*): 'Symmetrical systems, $\zeta = 0$, $\xi = 0$'.]

The curved boundaries on figure 1 (apart from the g.m. curve) were obtained by plotting either p_r, T_r- or T_r, x-diagrams of the critical lines depending on the boundary in question. The accuracy with which each boundary was determined varies. In figure 2 are shown all the points for which calculations were made. [Certain regions, particularly those in the vicinity of $\zeta = 0$ and those in the vicinity of the II–III boundary have been studied in greater detail since 1968.] Usually many calculations were made in each region over the whole composition range (at least twenty-nine values of x and usually more). Most of the calculations were made at points close to the boundaries where changes in the type of phase diagram occur.

Van Laar (1905) calculated the intersection of the double-point curve with the geometric-mean curve (g.m.) and our results correspond closely with his ($a_{22}/a_{11} = 2.89$ compared with our value of 2.887). [At this point a_{22}/a_{11} can be shown analytically to be exactly $(49 + 20\sqrt{6})/(17 + 12\sqrt{2}) = 2.88455$.] The geometric mean combining rule (22) was invariably used in the early work and p, T-phase diagrams in regions II and III were drawn, at least schematically, by van Laar (1905). [The reader who would study van Laar's voluminous papers should be warned that, while his mathematics was usually impeccable, the difficulties of numerical calculation in the days before electronic computers made it impossible to calculate accurately more than a few points. Consequently the curves drawn in his papers are frequently quantitatively, sometimes even qualitatively, wrong. Moreover, although many errors in figures in earlier papers are corrected in later papers, no mention is ever made of the fact that the earlier figures were wrong.]

(*a*) *Some calculated phase diagrams*

The simplest phase diagrams are found in regions close to the origin of figure 1 (class 1). When Λ or ζ or both have large values (positive or negative) the diagrams are more complicated and belong to class 2.

Critical lines are shown as dashed lines and pure vapour-pressure curves and three-phase lines as full lines. Because of the condition $b_{11} = b_{22}$, the vapour-pressure curve of component 2 (labelled 2) scales directly with the vapour-pressure curve of component 1 (labelled 1) by the

factor a_{22}/a_{11} $(= (1+\zeta)/(1-\zeta))$. An azeotrope line (labelled (AZ)) scales in the same way by the factor previously noted, $a(x^{AZ})/a_{11} = [2\Lambda - \zeta^2 - \Lambda^2]/[2\Lambda(1-\zeta)]$. The coordinates of the pure gas–liquid critical points C_1 and C_2 are (1, 1, 0) and $(a_{22}/a_{11}, a_{22}/a_{11}, 1)$.

For each of the classes of calculated phase diagrams there are corresponding examples in experimentally determined systems. Some of these are cited in subsequent pages; they are qualitatively similar, although of course none satisfy the special condition $\xi = 0$.

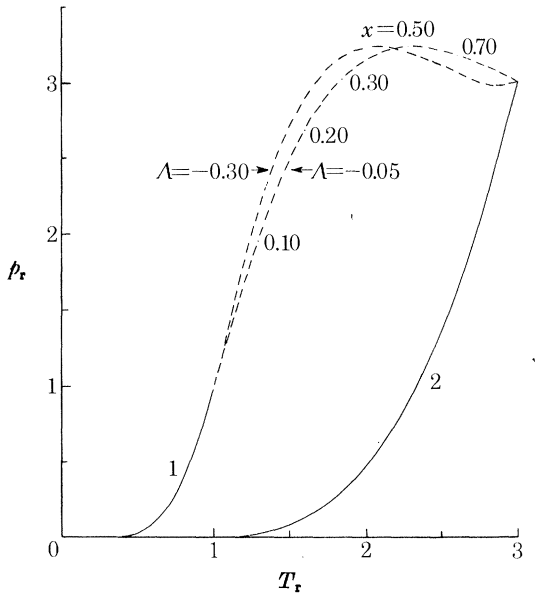

FIGURE 3. Reduced pressure–reduced temperature (p_r, T_r) projection of a type-I phase diagram ($\zeta = 0.50$; $\Lambda = -0.30, -0.05$). One critical line: C_1 to C_2 (G–L). In this and subsequent figures a dot on the dashed critical line is a calculated point for the mole fraction x indicated.

Class 1 diagrams

Type I: one critical line: C_1 to C_2 (G–L)

The simplest possible behaviour is found in region I of figure 1. Two examples are shown in figure 3. For clarity the same value of ζ has been chosen for both cases so that the vapour–pressure curves of the less volatile components in each mixture coincide. The composition is given at intervals along the critical line for $\Lambda = -0.05$.

For the diagrams in figure 3, when the gas–liquid critical line has positive slope it represents the locus of LCSTs and when the slope is negative the critical points are UCSTs. The phase behaviour is more clearly understood from the T_r, x-phase diagrams for a series of constant pressures given for $\Lambda = -0.05$ in figure 4. For $p_r < 1.00$ there are no critical lines at any value of T_r but there are two vapour-pressure curves. A typical example is shown at $p_r = 0.60$. At $p_r = p_1 = 1.00$ there is a critical point at $x = 0$, $T_r = 1$ (marked with a cross on the diagram), and the two-phase region becomes detached from the $x = 0$ side as the pressure is further increased in the succeeding cases. The diagram then shown a gas–liquid LCST at the minimum in the T_r, x-loop. At $p_r = p_2 = 3.00$, the two-phase region becomes detached from the $x = 1$ side as well. At $p_r > 3.00$, gas–liquid UCSTs appear as shown at $p_r = 3.15$. The LCST and UCST converge, as the pressure is increased, until at $p_r = 3.23$ they coincide. At still higher pressures there is no fluid–fluid equilibrium over the whole temperature range. (Restriction to the van der Waals equation does not allow the possibility of solid–fluid equilibrium.)

Within the dashed curve close to the origin of figure 1 the gas–liquid critical line has no maximum pressure; there are only LCSTs in this case and a two-phase region can exist only for pressures less than $p_r = p_2$. The critical line for $A = -0.30$ (figure 3) has a slight dip close to C_2; this feature is present in some diagrams close to regions of azeotropy.

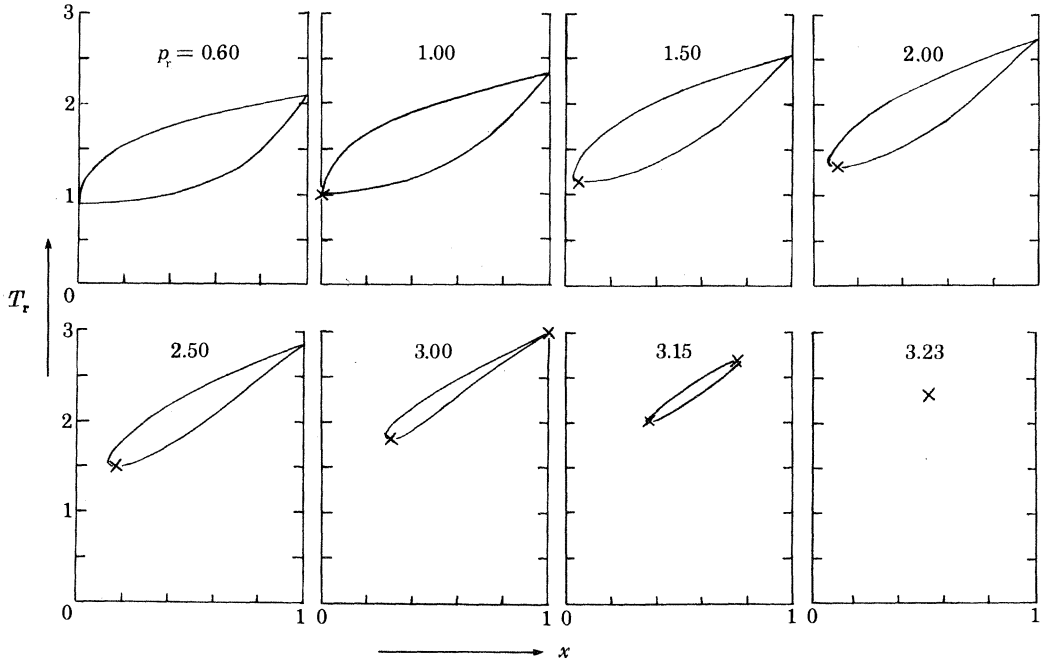

FIGURE 4. Reduced temperature–mole fraction (T_r,x) isobars for the type-I system of figure 3 ($\zeta = 0.50$, $A = -0.05$).

Many experimentally determined systems are of the simple type I, usually, although not necessarily, with a maximum pressure along the critical line, for example, $CO_2 + O_2$, Ar + Kr, $N_2 + O_2$, $C_2H_6 + n\text{-}C_7H_{16}$. [Some of these have positive heats of mixing and one suspects that, if the solid phase had not intervened, upper critical solution phenomena would have been observed at low temperature; if so, such a system is really type II.] References for these and subsequent examples may be found in reviews by Rowlinson (1959, 1969) and by Schneider (1966).

[For certain values of ζ and A it is possible to have type I (or II) systems where the critical line starting at C_2 goes initially to higher temperature and pressure before bending around to go to C_1; this means that liquid–liquid phase separation occurs at temperatures higher than the gas–liquid critical temperature of either pure component, so Scott (1973) has suggested that this phenomenon be called 'gas–gas immiscibility of the third kind'. Examples are $HCl + (C_2H_5)_2O$ and cycloheptane + tetraethylsilane (Hicks & Young 1971).

[It is a feature of van der Waals-like equations of state that at C_1 the initial slopes dT/dx_2 and dp/dx_2 along the critical line can be positive or negative, but that a positive dT/dx_2 cannot be associated with a negative dp/dx_2. (Equivalent conditions apply at C_2.) At least one experimental system, $SO_2 + CH_3Cl$, appears to violate this condition.]

Type I-A: the same as type I, with the addition of a negative azeotrope

As mentioned in §3, negative azeotropy first appears at the boundary $a_{12} = a_{22}$ ($A = -\zeta$). An example of a phase diagram in region I-A is shown in figure 5. The cusp in the critical

line where it joins the azeotrope line is clearly demonstrated. The slopes of both branches of the critical line are positive and imply LCSTs.

T_r, x-diagrams for a series of pressures are given for this system in figure 6. For $p_r < p_1 = 1.00$ there are no critical points (as in region I), and the azeotrope vapour–liquid diagram spans the whole composition range. At pressures greater than $p_r = 1.00$ an LCST appears at low composition, and greater than $p_r = p_2 = 1.222$ a second LCST appears on the other branch. Finally at $p_r = 1.295$ the two critical points both occur at the azeotropic point. This is not the only way in which an azeotrope can disappear in region I-A; another way will be demonstrated as an example in region V-A. Experimentally it has been shown that the azeotrope line

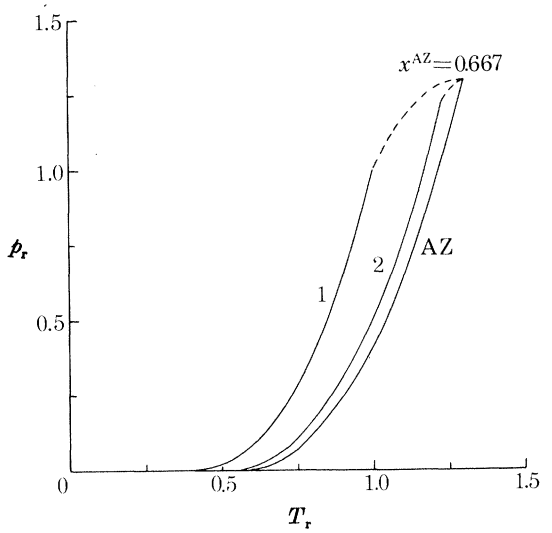

FIGURE 5. p_r, T_r-projection of a type-I-A phase diagram ($\zeta = 0.10$, $\Lambda = -0.30$). One critical line, C_1 to C_2 (G–L); one negative azeotrope line.

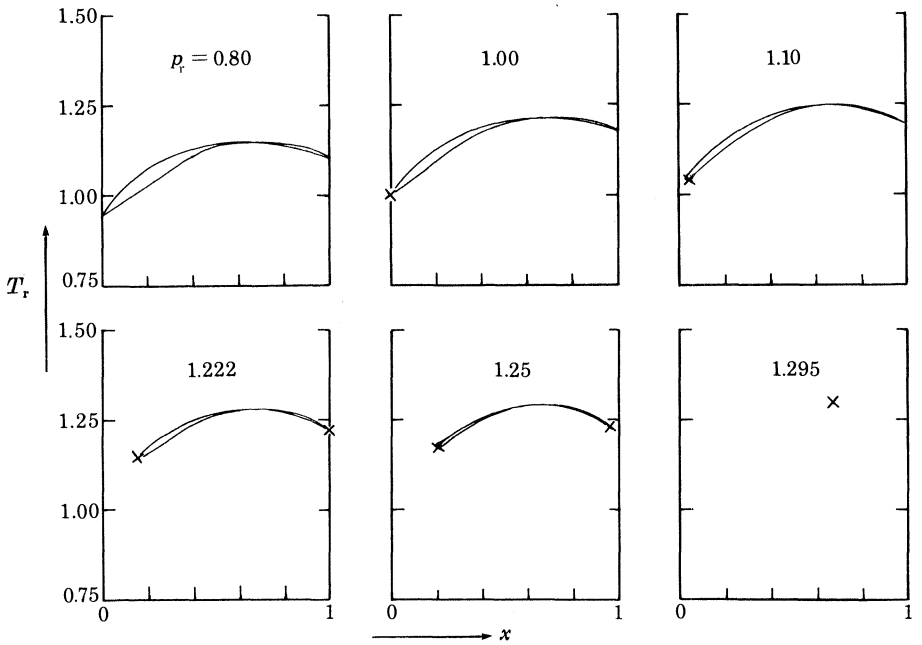

FIGURE 6. T_r, x-isobars for the type-I-A system of figure 5 ($\zeta = 0.10$, $\Lambda = -0.30$).

frequently disappears at $x = 0$ or $x = 1$; this cannot happen for $\xi = 0$ because the azeotropic composition is independent of pressure and temperature, as we saw in a preceding section.

An example of type I-A behaviour is the experimental phase diagram for the system $HCl + (CH_3)_2O$.

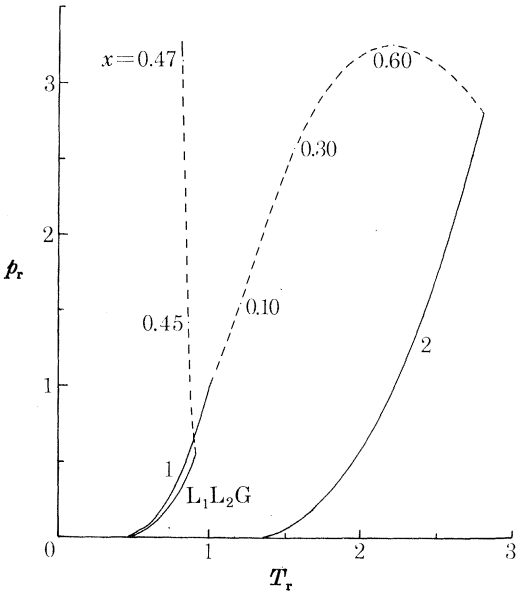

FIGURE 7. p_r, T_r-projection for a type-II system ($\zeta = 0.473$, $\Lambda = 0.105$). Two critical lines: C_1 to C_2 (G–L); C_m to UCEP (L–L; $p_r = 0.553$, $T_r = 0.911$, $x^G = 0.0072$, $V_r^G = V_m^G/b = 9.56$, $x_c^{LL} = 0.424$, $V_r^{LL} = V_m^{LL}/b = 1.25$).

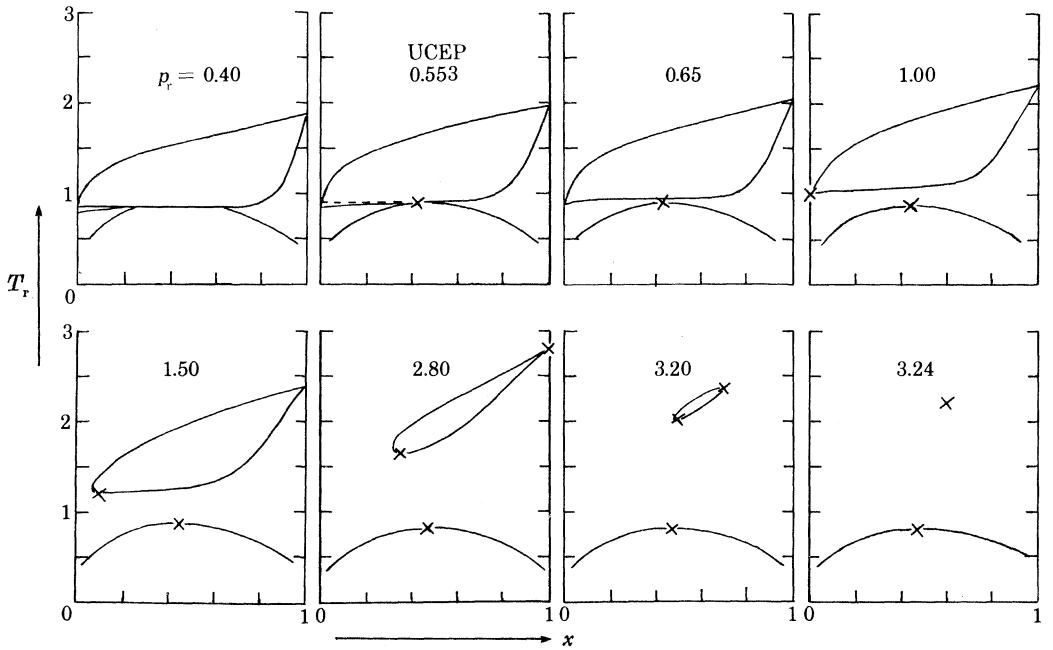

FIGURE 8. T_r, x-isobars for the type-II system of figure 7 ($\zeta = 0.473$, $\Lambda = 0.105$).

Type II: two critical lines: C_1 to C_2 (G–L), C_m to UCEP (L–L)

An important feature of figure 1 is that for positive values of Λ, liquid–liquid phase separation must always occur at a sufficiently low temperature (although in experimental systems the formation of a solid phase may hide this). In region II the phase behaviour is similar to that

of region I but as seen in figure 7 there is a second critical line, the locus of liquid–liquid UCSTs starting from $C_m(T_m^\infty, \infty, \frac{1}{2})$. This critical line continues to low pressure until it is terminated at a UCEP where a gaseous third phase appears. A three-phase line (L_1L_2G) continues from the UCEP to $p_r = T_r = 0$. The gas–liquid critical line can be interpreted as in region I.

A series of T_r, x-diagrams for this system are given in figure 8. The three-phase line always lies between the vapour-pressure curves of the two pure components. This is illustrated for $p_r = 0.40$. For small T_r two liquids are in equilibrium over most of the composition range. The two liquid phases are in equilibrium with a gaseous third phase at the horizontal three-phase line. The temperature along the liquid–liquid critical line shown in figure 7 decreases with increasing pressure. However, in other cases, the temperature along this critical line first decreases and then increases with increasing pressure. Obviously, whenever T_m^∞, the temperature of the 'liquid–liquid' critical point at infinite pressure, is greater than the temperature of the UCEP, there must be some pressure range over which the temperature along the liquid–liquid critical line increases.

An experimental example of a type-II phase diagram is the system $CO_2 + n\text{-}C_8H_{18}$.

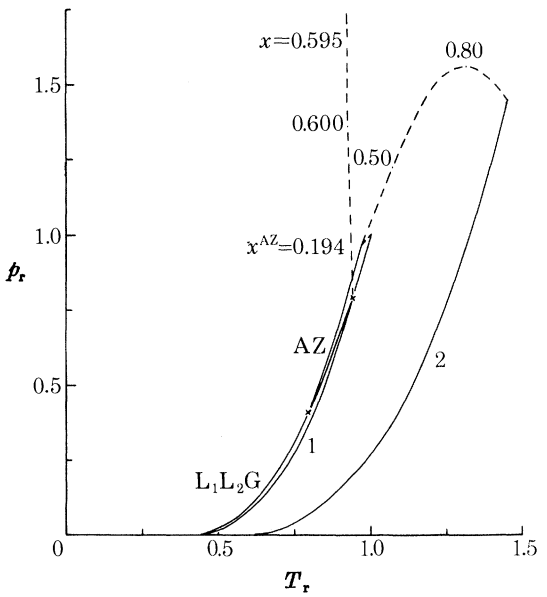

FIGURE 9. p_r, T_r-projection for a type-II-A system ($\zeta = 0.184$, $\Lambda = 0.300$). Two critical lines: C_1 to C_2 (G–L); C_m to UCEP (L–L; $p_r = 0.795$, $T_r = 0.941$, $x^G = 0.313$, $V_r^G = 5.53$, $x_c^{LL} = 0.605$, $V_r^{LL} = 1.633$). One positive azeotrope line (which joins two three-phase lines at $p_r = 0.41$, $T_r = 0.79$).

Type II-A: the same as type II, with the addition of a positive azeotrope

Positive azeotropy has already been shown to begin at the boundary $a_{12} = a_{11}(\Lambda = \zeta)$ in figure 1. True positive azeotropic behaviour exists only in region II-A and an example is given in figure 9. The azeotropic effect is small here; the values $\Lambda = 0.30$ and $\zeta = 0.184$ were chosen so that some of the other features would be clearly shown. Positive azeotropy is always limited azeotropy because the azeotrope line must disappear at small pressures at an endpoint (marked with a cross, $\times$) where it intersects a three-phase line (SLG or L_1L_2G in real systems; only L_1L_2G when the van der Waals equation is used). If Λ were decreased, with ζ constant, this endpoint would occur at still smaller pressures and it would be difficult to locate. For this example, the UCEP is, accidentally, very close to the vapour–pressure curve, 1, and is also

marked with a cross. Calculated T_r, x-diagrams are given for this example in figure 10. Since the azeotropic and three-phase lines are so close to the vapour-pressure curve of component 1, details are given in enlargements of the region around the azeotropic composition.

The temperature along the branch of the three-phase line that exists below the azeotrope endpoint is lower than that of either of the one-component vapour-pressure curves. At these

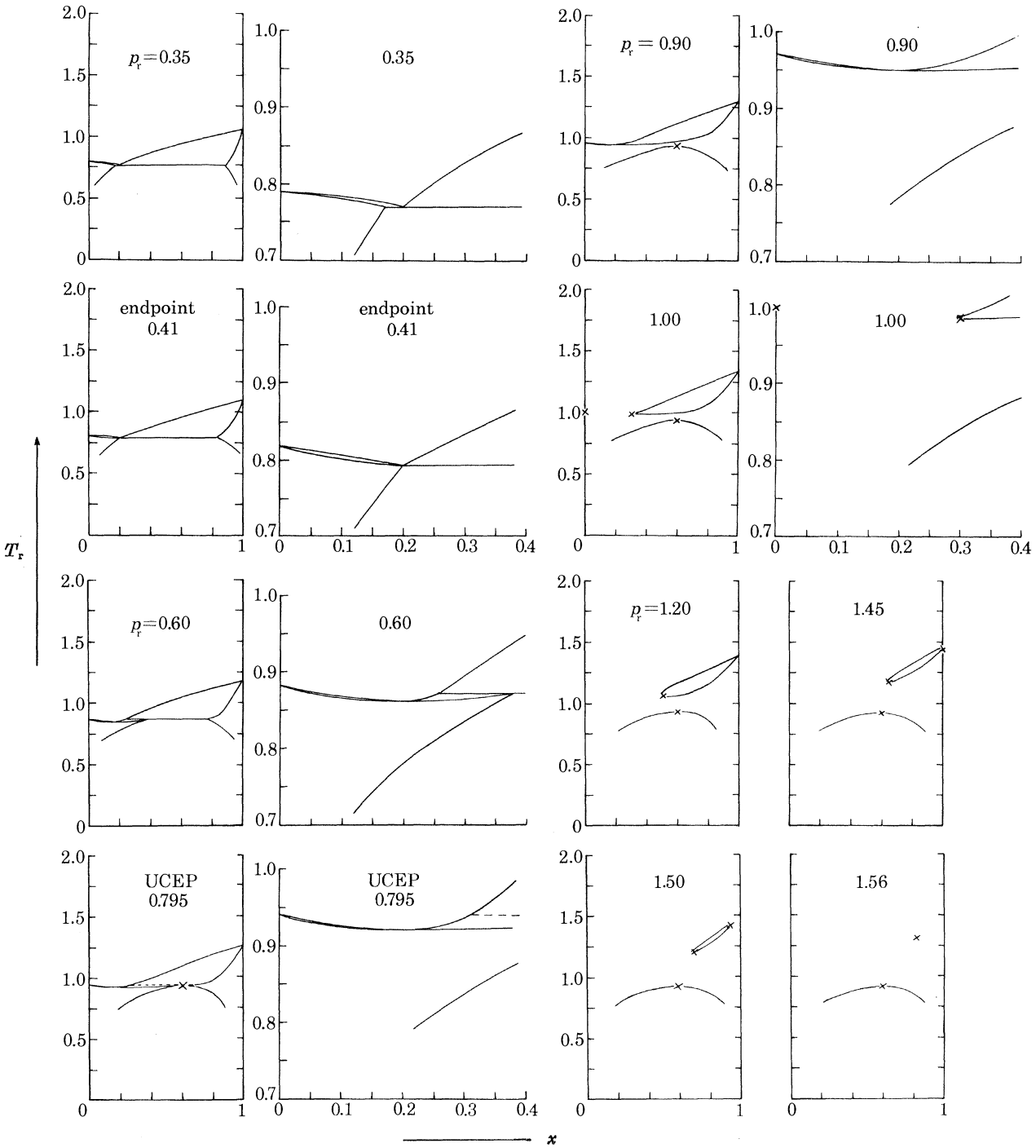

FIGURE 10. T_r, x-isobars for the type-II-A system of figure 9 ($\zeta = 0.184$, $\Lambda = 0.300$).

low pressures, such as at $p_r = 0.35$ (figure 10), there is a constant-boiling mixture, the liquid phase being heterogeneous (for example, steam distillation). This behaviour is described as 'heteroazeotropy'.

An experimental example with positive azeotropy giving a type II-A phase diagram is the system $CO_2 + C_2H_6$, although the low temperature C_m–UCEP critical line is not seen (presumably hidden below the melting curve).

Class 2 diagrams

In this section the possible phase diagrams in which there is no continuous stable critical line joining the gas–liquid critical points (C_1 and C_2) of the two components will be examined. They will be presented roughly in order of decreasing Λ.

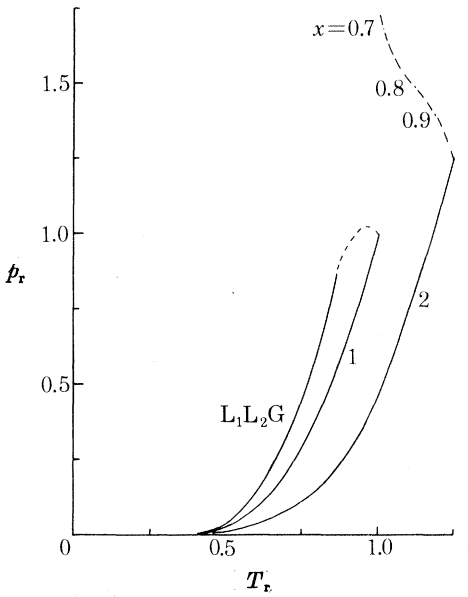

FIGURE 11. p_r, T_r-projection for a type-III-HA system ($\zeta = 0.111$, $\Lambda = 0.444$). Two critical lines: C_1 to UCEP (G–L, $x_c \approx 0.33$); C_m to C_2.

Type III-HA: two critical lines: C_1 to UCEP (G–L), C_m to C_2 (L–L to G–L)

A three-phase line runs from a UCEP to $p = 0$, $T = 0$ at lower temperatures than the one-component vapour-pressure curves, producing 'heterozaeotrope' behaviour.

At the boundary between regions II-A and III-HA the low-temperature liquid–liquid UCST critical line moves to high temperature and connects with the gas–liquid critical line at the end of the azeotropic curve. The result is that in region III-HA the critical line originating at C_2 continues to C_m. The critical line beginning at C_1 ends at a UCEP.

Examples from region III-HA and the subregion III-HA_m are given in figures 11 and 13. Above the dashed line labelled $T_m^\infty = T_2$ on figure 1, the critical temperature at infinite pressure is greater than the gas–liquid critical temperature of the less volatile component 2. In this region the critical line originating at C_2 can increase monotonically in temperature as the pressure increases or it can have a minimum temperature. (The maximum pressure in the C_1–UCEP line does not appear in all III-HA diagrams; for example at $\zeta = 0.30$, $\Lambda = 0.40$, p_r increases monotonically from UCEP to C_1.)

In the regions III-HA and III-HA$_m$ the three-phase line lies at a lower temperature than the vapour-pressure curve of the pure component 1 and continues up to the gas–liquid critical line where it ends at a UCEP. This example might be called 'absolute heteroazeotropy' by analogy with the azeotropy nomenclature. A series of T_r,x-diagrams is given in figure 12 for the p_r,T_r-diagram in figure 11. Figure 13 shows an example close to the boundary between regions III-HA$_m$ and II-A. The subscript m on the region label implies that a maximum and a minimum appear in the gas–liquid critical curve before it continues to C$_m$.

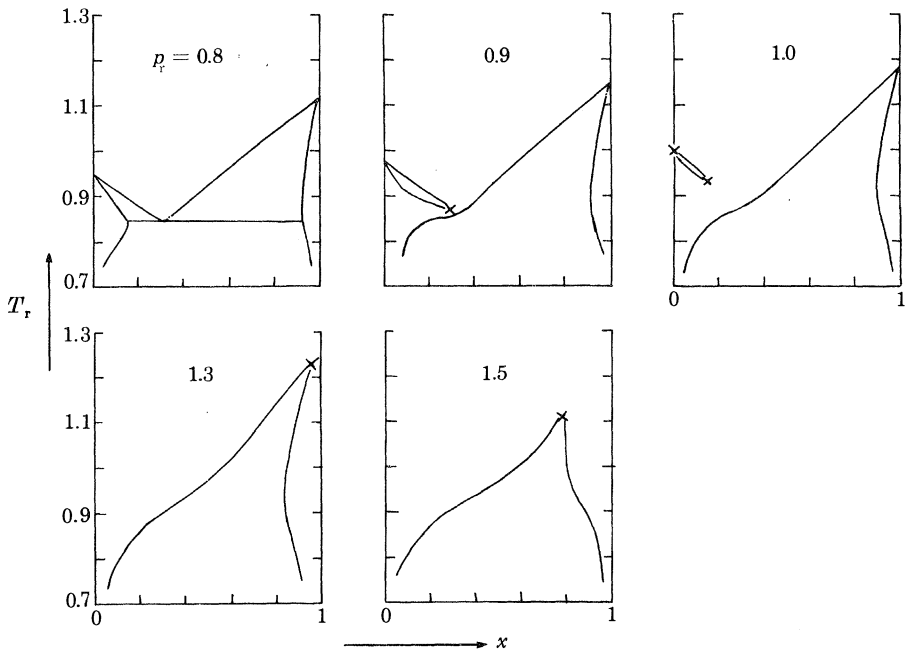

FIGURE 12. T_r,x-isobars for the type-III-HA system of figure 11 ($\zeta = 0.111$, $\Lambda = 0.444$).

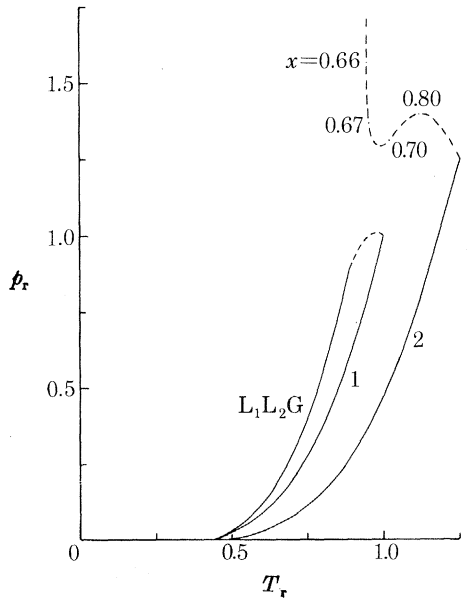

FIGURE 13. p_r,T_r-projection for a type-III-HA$_m$ system ($\zeta = 0.111$, $\Lambda = 0.400$). Two critical lines: C$_1$ to UCEP; C$_m$ to minimum pressure, minimum pressure to maximum pressure, maximum pressure to C$_2$.

[At the time the foregoing was written, in 1968, we were apparently convinced that ordinary azeotropy ceased at the boundary between II–A and what is labelled III–HA. This does not now seem to be required. Whenever $\Lambda > |\zeta|$ there is an azeotrope line that ends on a critical line. The question is whether this point lies on a stable, a metastable, or an unstable part of the critical line; only if this part of the critical line is stable will the azeotrope appear in the equilibrium diagram.

[Whenever there is a continuous critical line from one gas–liquid critical point to the other (C_1 to C_2), it is (except for type-IV systems to be discussed later) stable over its entire length; consequently there must be a stable azeotrope line of non zero length in all systems belonging to region II-A. The situation in the region labelled III-HA is less clear. The azeotrope line must end on the critical line that starts at C_1, but its end could be at a point on a metastable or unstable extension beyond the UCEP. It now seems to us that there must be a region adjacent to the II-A and III boundaries in which the low pressure heteroazeotrope diagram (for example, figure 10, $p_r = 0.35$) changes to an azeotrope diagram (for example, figure 10, $p_r = 0.60$) followed at higher pressures by a splitting of the azeotropic diagram into two separate loops with critical points. At a sufficient distance from these boundaries, the azeotrope line will shrink to zero and only heteroazeotropic phase diagrams (for example, figure 11) will exist. To determine the extent of this region will require some detailed calculations that we have not yet made.]

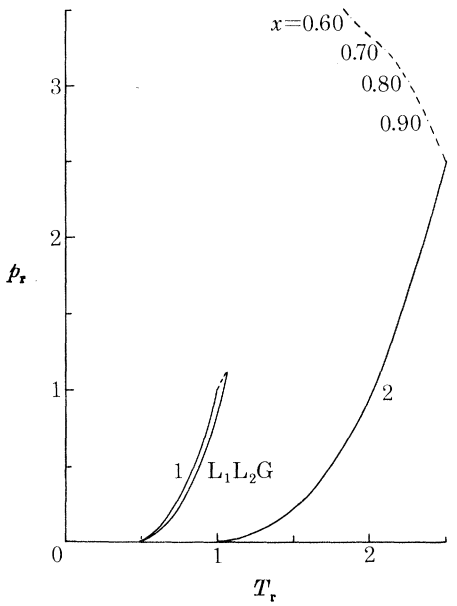

FIGURE 14. p_r, T_r-projection of a type-III phase diagram ($\zeta = 0.428$, $\Lambda = 0.257$). Two critical lines: C_1 to UCEP (G–L; $p_r = 1.108$, $T_r = 1.055$, $x_c^{GL} = 0.060$, $V_r^{GL} = 2.87$, $x^L = 0.932$, $V_r^L = 1.18$); C_m to C_2.

Type III: the same as type III-HA with the three-phase line lying between the two one-component vapour-pressure curves

When the boundary $a_{12} = a_{11}$ ($\Lambda = \zeta$) is crossed from region III-HA into III, the three-phase line changes its position relative to the pure vapour-pressure curve of component 1, moving to a higher temperature between the curves for components 1 and 2. Figures 14 and 15 show an example from region III and how the three-phase line always ends at temperatures

and pressures greater than those at C_1, a UCEP. Above the UCEP the phase behaviour is exactly the same as in region III-HA.

The mutual solubility of the two components increases when passing from region III into III_m at constant ζ. Figure 16 illustrates this trend; the insolubility at high pressures has moved to lower temperatures. Again the subscript m on the region label implies a maximum and a minimum in the critical line. At pressures between the maximum and minimum pressures there are two regions in the T_r, x-phase diagrams as shown in figure 17. At the minimum pressure the vapour–liquid region separates from the liquid–liquid boundary. At these pressures and temperatures, however, the 'liquid' and 'gas' phases sometimes have very similar densities

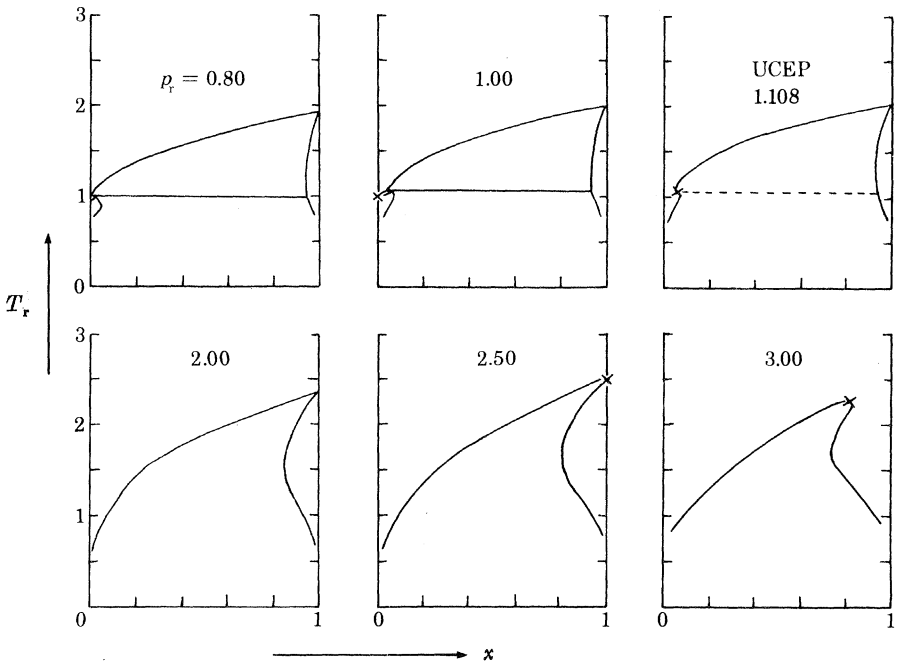

FIGURE 15. T_r, x-isobars for the type-III system of figure 14 ($\zeta = 0.428$, $\Lambda = 0.257$).

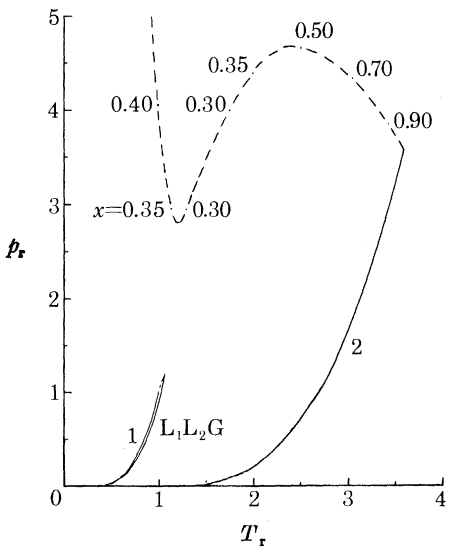

FIGURE 16. p_r, T_r-projection of a type-III_m phase diagram ($\zeta = 0.565$, $\Lambda = 0.0869$). Two critical lines: C_1 to UCEP (G–L; $p_r = 1.203$, $T_r = 1.069$, $x_c^{GL} = 0.0176$, $V_r^{GL} = 2.562$, $x^L = 0.630$, $V_r^L = 1.154$); C_m to C_2.

and the distinction is not clear. The 'gas–liquid' region disappears at sufficiently high pressures but the 'liquid–liquid' boundary continues to C_m.

Another example in region III_m, at a lower value of Λ, is given in figures 18 and 19. Here the minimum in the 'gas–liquid' critical curve is near p_1. The 'liquid–liquid' UCST detaches from the 'gas–liquid' region before the UCEP is reached. Figure 19 shows the 'hour-glass'

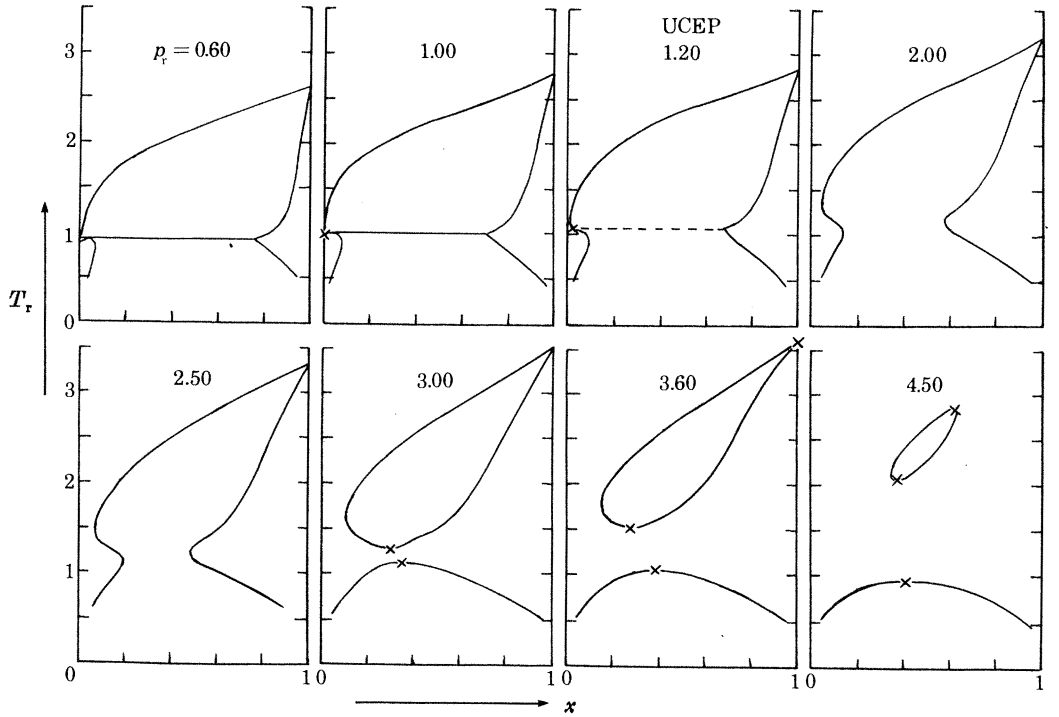

FIGURE 17. T_r, x-isobars for the type-III_m system of figure 16 ($\zeta = 0.565$, $\Lambda = 0.0869$).

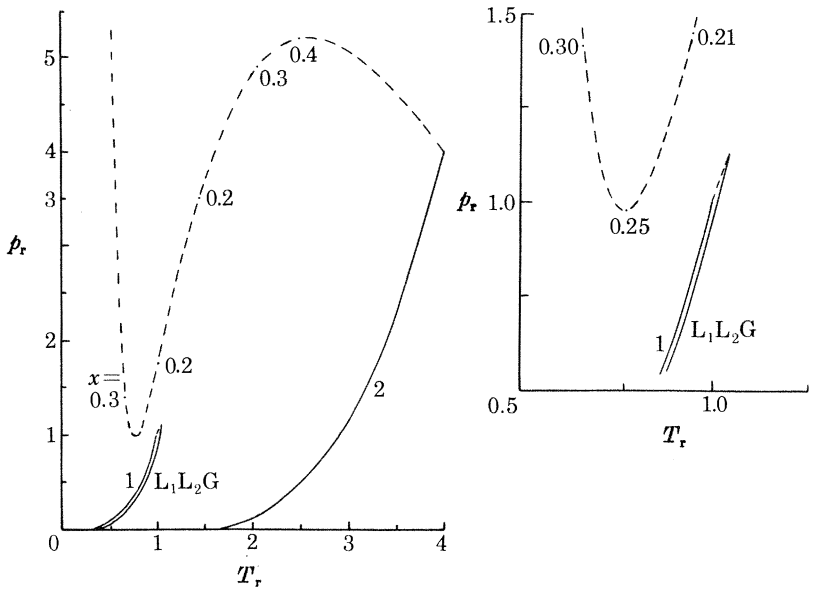

FIGURE 18. p_r, T_r-projection of a type-III_m phase diagram ($\zeta = 0.60$, $\Lambda = 0.040$). An enlargement of the region around C_1 is also shown. (The UCEP is at $p_r = 1.127$, $T_r = 1.041$, $x_c^{GL} = 0.0071$, $V_r^{GL} = 2.058$, $x^L = 0.462$, $V_r^L = 1.179$).

shape of the liquid–liquid two-phase region below the three-phase line. At $p_r = 1.0$ (shown in figure 19) the two parts have separated leaving a low-temperature UCST and a liquid–liquid LCST. Examples giving type-III or III_m phase diagrams are the systems He + Xe, Ne + Kr, $CH_4 + n\text{-}C_7H_{16}$, $CO_2 + n\text{-}C_{13}H_{28}$.

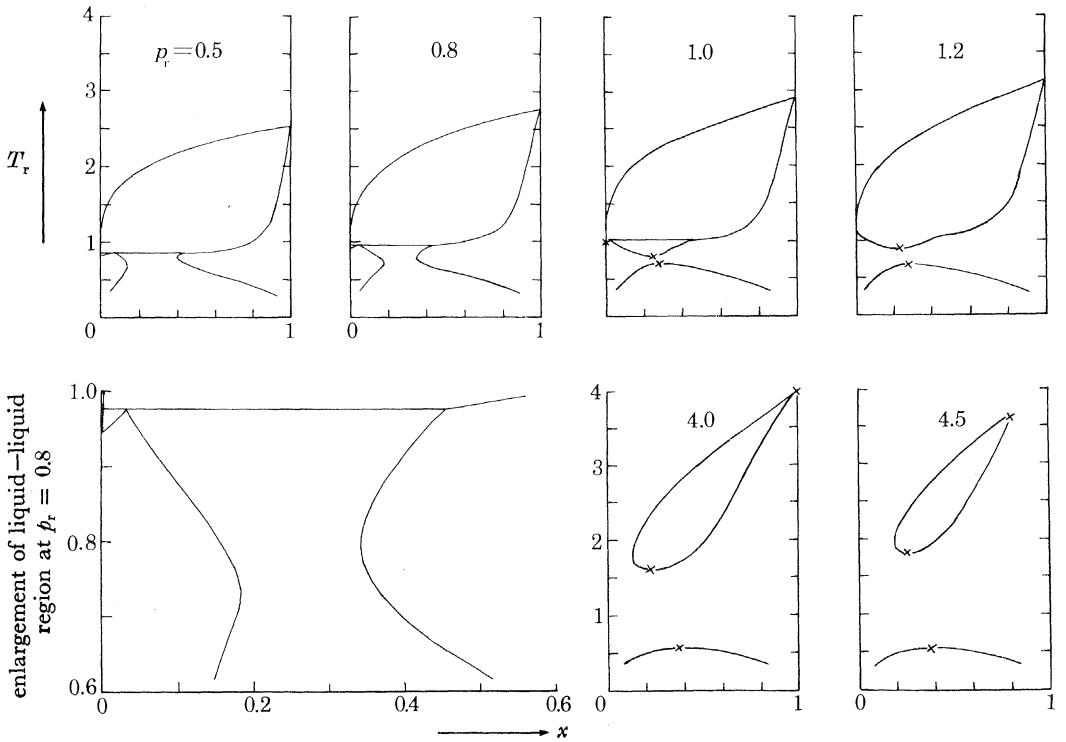

FIGURE 19. T_r, x-isobars for the type-III_m system of figure 18 ($\zeta = 0.60$, $\Lambda = 0.040$).

In all of the two regions and two subregions labelled III (III-HA, III-HA_m, III and III_m), the three-phase line is stable from $p_r = 0, T_r = 0$ up to the gas–liquid critical line. This type of behaviour has been called *absolute immiscibility* by Davenport & Rowlinson (1963). Phase diagrams in region I, where there is no three-phase equilibrium, exhibit *complete miscibility*. The remaining three regions to be described are cases of *limited miscibility*, where the three-phase line exists over only part of the liquid range, as in the simpler types II and II–A diagrams.

Type IV: three critical lines. C_1 to UCEP (G–L), LCEP to C_2 (L–L to G–L) and C_m to UCEP (L–L)

Region IV typifies the liquid–liquid UCST–LCST behaviour found in the systems methane + 1-hexene (Davenport *et al.* 1966) and benzene + polyisobutylene (Freeman & Rowlinson 1960). Three more hydrocarbon solutes (3,3-dimethylpentane, 2,3-dimethyl-1-butene, and 2-methyl-1-pentene) have been found to show similar type-IV behaviour with methane [Scott & van Konynenburg 1970].

A calculated phase diagram for region IV is shown in figure 20. This type of diagram results when the minimum in the critical line going from C_2 to C_m appearing in diagrams for region III_m (for example, figure 19) has crossed the three-phase line and divided it into two parts. When the 'gas–liquid' critical line that originates at C_2 reaches the region of mixtures rich in

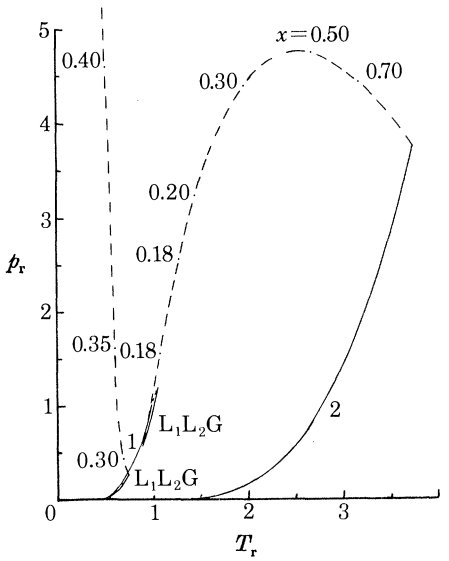

FIGURE 20. p_r, T_r-projection of a type-IV phase diagram ($\zeta = 0.5795$, $\Lambda = 0.0446$). Three critical lines: C_1 to UCEP (G–L; $p_r = 1.205$, $T_r = 1.066$, $x_c^{GL} = 0.0148$, $V_r^{GL} = 2.487$, $x^L = 0.372$, $V_r^L = 1.236$); LCEP (L–L; $p_r = 0.554$, $T_r = 0.885$, $x^G = 0.0003$, $V_r^G = 8.91$, $x_c^{LL} = 0.218$, $V_r^{LL} = 1.261$) to C_2; C_m to UCEP (L–L; $p_r = 0.241$, $T_r = 0.738$, $x^G < 10^{-4}$, $V_r^G \approx 20.3$, $x_c^{LL} = 0.275$, $V_r^{LL} = 1.175$).

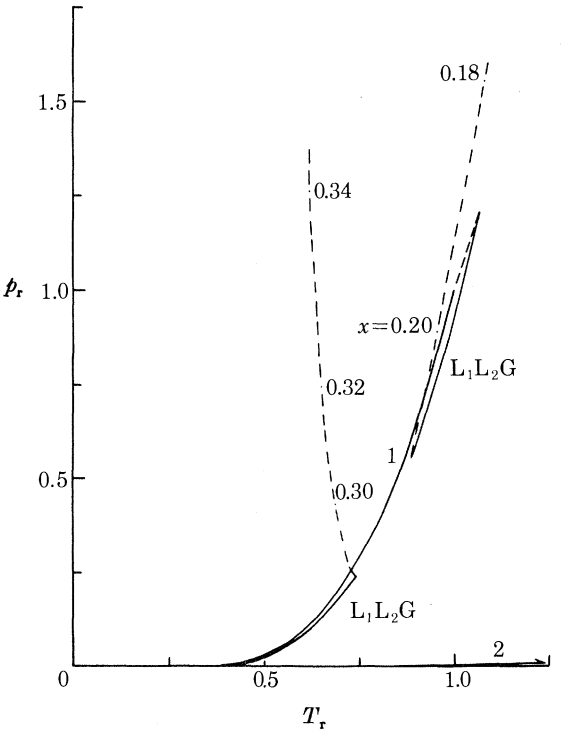

FIGURE 21. Enlargement of the region around the three critical endpoints of the system of figure 20 ($\zeta = 0.5795$, $\Lambda = 0.0446$).

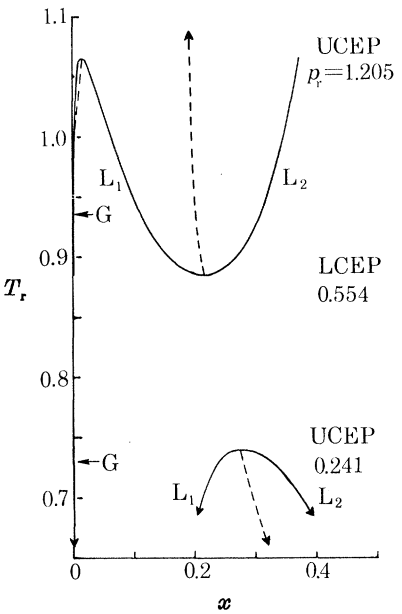

FIGURE 22. T_r, x-projection of the two three-phase lines occurring in the type-IV system of figures 20 and 21 ($\zeta = 0.5795$, $\Lambda = 0.0446$).

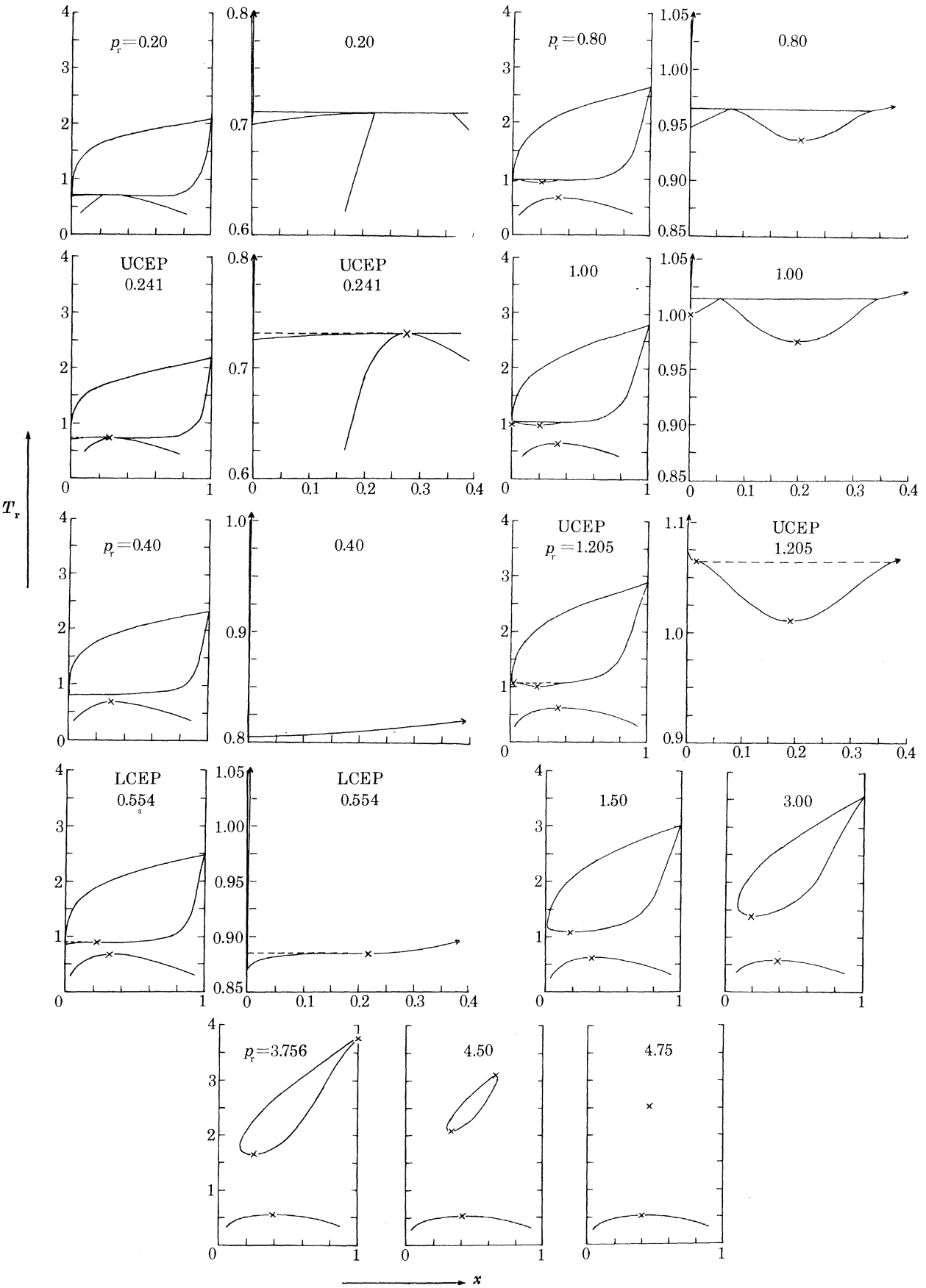

FIGURE 23. T_r, x-isobars for the type-IV system of figures 20–22 ($\zeta = 0.5795$, $\Lambda = 0.0446$).

PHILOSOPHICAL TRANSACTIONS OF THE ROYAL SOCIETY A MATHEMATICAL, PHYSICAL & ENGINEERING SCIENCES

component 1 (small x), it is essentially a liquid–liquid LCST line which terminates at the three-phase line at a LCEP. The liquid–liquid UCST line starts from C_m and ends at a UCEP just as in region II. The region around the critical endpoints is magnified in figure 21.

The three-phase lines are better understood by plotting the temperature dependence of the composition of the three phases in equilibrium as in figure 22. The pressure is varying with the temperature on this diagram and, as can be seen from figures 20 and 21, is only slightly lower than the vapour-pressure of the pure component 1 at the same temperature. If pressure were plotted instead of temperature, the diagram would have substantially the same form. The arrowheads on the L_1, L_2 and G curves at low temperature mean that these lines continue to $T_r = 0$. Rowlinson & Freeman (1961) have published the experimental curve for ethane with a hydrocarbon polymer, corresponding to the upper half of figure 22, and the same general features are evident. [The three-phase line for the system methane + 2,3-dimethylbutane (Creek *et al.* 1977) is also representative of this type of phase diagram.] The low-temperature UCSTs in these systems presumably lie below solid boundaries.

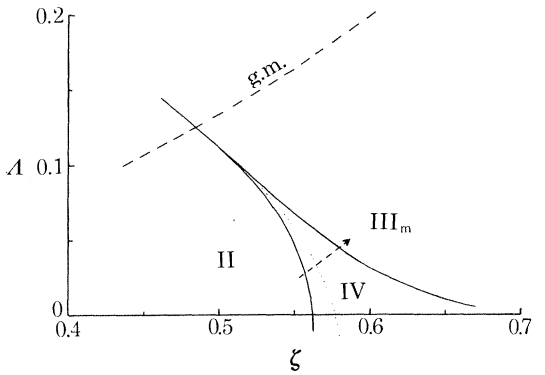

FIGURE 24. Enlarged view of the area around region IV of figure 1. The dashed arrow through region IV is explained in the text.

A series of T_r, x-diagrams at various constant pressures for the system in figure 20 is shown in figure 23. For some of these an enlargement of the region about $T_r = 1$, $x = 0$ is given.

The van der Waals model clearly shows a continuous variation in behaviour similar to that in the following series of mixtures (Davenport & Rowlinson 1963).

system		phase behaviour
CH_4 + *n*-pentane	type II	complete miscibility
CH_4 + *n*-hexane	type IV	limited miscibility
CH_4 + *n*-heptane	type III	absolute immiscibility

In the first two mixtures a metastable low-temperature UCEP is presumed to lie below a solid boundary. [The shape of the melting curve in the system methane + *n*-hexane offers strong evidence for a metastable UCST near $T = 150$ K, $x_{CH_4} = 0.8$ (Dickinson *et al.* 1973).]

Figure 24 gives an enlarged view of the area around region IV of figure 1. There are many paths that can be taken to go from region II to region IV to region III but all will show the decrease in miscibility in a similar manner. One of these paths is illustrated by a dashed arrow in the figure. Critical endpoints have been calculated for systems along this line and their locus is shown in figure 25. Here the temperatures of the critical endpoints are plotted against the ratio $a_{22}/a_{11} = T_2/T_1$. The curve at temperatures greater than T_1 represents the high-temperature UCEP, which begins at the boundary between regions II and IV and continues

into region III. [This is a line of *upper* critical endpoints, because they lie at the upper end (T and p) of a three-phase line; however, as a careful study of figure 23 will show, the critical line that ends at such a UCEP is a line of *lower* critical solution temperatures (LCSTs).] The curve representing the locus of LCEPs begins at the same point as the high-temperature UCEPs and decreases in temperature through region IV. The lowest curve belongs to the low-temperature UCEP; it runs from region II through region IV and steadily increases in temperature until it joins smoothly to the LCEP curve at the boundary between regions IV and III.

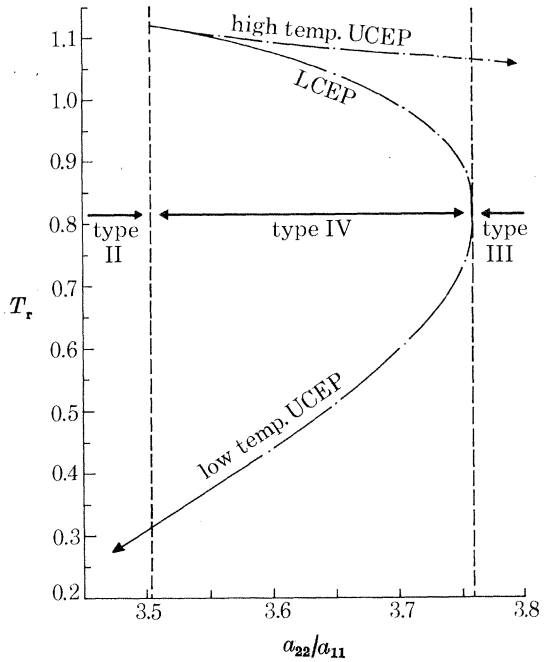

FIGURE 25. The locus of critical endpoints for systems along the arrow drawn in figure 24. The points along the curve represent calculated endpoints.

[At the boundary between regions II and IV the point where the two critical endpoint lines end in a cusp (figure 25) is a 'tricritical point'. In principle a tricritical point is a point at which three coexisting phases simultaneously become identical (Widom 1973; Griffiths 1974); however, in unsymmetrical fluid systems a path along which three phases become identical is not experimentally attainable in a closed system. Moreover, in the absence of special symmetry the phase rule forbids tricritical points in systems of fewer than three components. In terms of figure 25 this restriction arises from the fact that one cannot vary the ratio a_{22}/a_{11} continuously in a set of binary mixtures.

[However we have shown (van Konynenburg 1968; Scott & van Konynenburg 1970) that phase equilibrium in ternary mixtures of hydrocarbons (for example, methane with a pair of higher alkanes) can be reasonably well represented as that in a set of 'quasibinary' mixtures in which the 'solute' (actually a pair of very similar alkanes in varying proportions) may have a continuous spectrum of thermodynamic properties. In such a quasibinary system the ratio a_{22}/a_{11} can be continuously varied and a tricritical point approached as closely as experimental precision permits. Creek *et al.* (1977) have found such a tricritical point in two systems: methane + (*n*-pentane + 2,3-dimethylbutane) and methane + (2,2-dimethylbutane + 2,3-dimethylbutane). Their experimental plots of the critical endpoint curves (temperature

against the composition of the 'solute' mixture are qualitatively the same as the upper half of figure 25.]

[The boundary separating regions II and IV and that separating regions IV and III (on the master diagram figure 1) intersect exactly at the geometric mean line ($\zeta = (10\sqrt{6} - 6\sqrt{2})/33 = 0.48514$, $\Lambda = 0.12556$), a feature known to van Laar. In 1968 we believed (as we think van Laar believed for the somewhat analogous ξ, ζ diagram for the geometric mean) that beyond this point a single boundary defined a direct transition from type II to type III. In response to a query from R. B. Griffiths and J. C. Wheeler we tardily re-examined this point and found that the two boundaries *crossed* at the geometric mean line and that there is a very narrow region separating type II from type III. In the meantime Furman & Griffiths (1978) had made similar calculations for the van der Waals binary mixture and had reached identical conclusions.

[Beyond the geometric mean line the two boundaries define a new region, which we may call type IV*, so narrow that it is almost certainly of no practical importance. Without the precision of modern high speed computers the separation could not even have been determined; at $\zeta = 0.30$ 0.15, and 0.00 the difference in Λ between the two boundaries is approximately $\Delta\Lambda = 1 \times 10^{-5}$, 2×10^{-6} and 5×10^{-7}, respectively. Type-IV* and type-IV phase diagrams differ in the connectivity of the three critical lines. In type IV the three are C_1 to UCEP (higher), C_m to UCEP (lower), and C_2 to LCEP (intermediate); in type IV* it is C_m that connects with the higher UCEP and C_1 that connects to the lower UCEP while C_2 still is joined to the intermediate LCEP. The diagram corresponding to figure 25 is reversed; the tricritical point cusp is at the boundary between IV* and III at higher a_{22}/a_{11} (higher Λ and ζ). For other simple van der Waals-like equations of state, the intersection of the two boundaries (i.e. the change from IV to IV*) does not necessarily occur at the geometric mean line, but the IV* region is again very narrow.]

Type V: two critical lines: C_1 to UCEP (G–L), LCEP to C_2 (L–L to G–L)

At the arithmetic mean line (a.m.) or abscissa in figure 1 the low-temperature UCST phenomenon disappears at $T_r = 0$. At this boundary between regions IV and V only the three-phase line close to C_1 remains. An example for the arithmetic mean is given in figure 26, with an enlargement of the region around the three-phase line in figure 27. [The example of type V given in figures 26 and 27 is for a system that actually lies on the boundary between type IV and type V ($\Lambda = 0$), but the behaviour is qualitatively like that of any type-V system. Calculated T_r, x-phase diagrams at different p_r for this system were given in the thesis, but, since they are almost indistinguishable from those shown in figure 23 (except of course for the absence of the low-temperature liquid–liquid equilibria), they are omitted here.]

As shown in figure 25 an LCEP can lie at temperatures above $T_r = 1$. A p_r, T_r-diagram is given in figure 28 as an example of this behaviour for a system from region V. Only the area around C_1 is shown.

Examples of type-V phase diagrams include ethane + ethanol, carbon dioxide + nitrobenzene, and methane + *n*-hexane, but, as indicated above, some of these are probably really type IV with the C_m-UCEP critical line hidden below the melting curve.

PHILOSOPHICAL TRANSACTIONS OF THE ROYAL SOCIETY A MATHEMATICAL, PHYSICAL & ENGINEERING SCIENCES

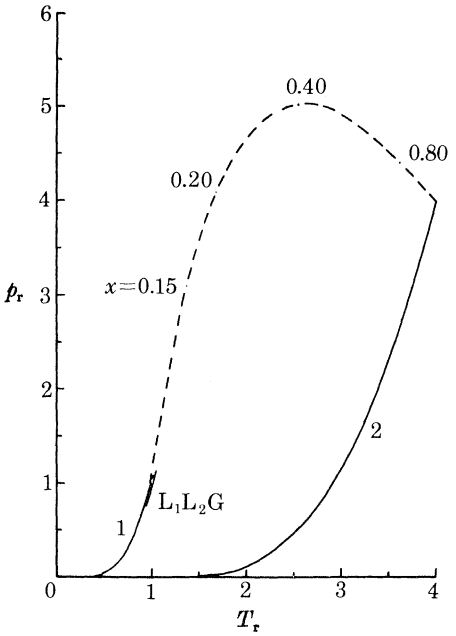

FIGURE 26. p_r, T_r-projection of a type-V phase diagram ($\zeta = 0.6, \Lambda = 0.0$). Two critical lines: C_1 to UCEP (G–L; $p_r = 1.1313$, $T_r = 1.0417$, $x_c^{GL} = 0.0068$, $V_r^{GL} = 2.618$, $x^L = 0.2658$, $V_r^L = 1.265$); LCEP (L–L; $p_r = 0.745$, $T_r = 0.942$, $x^G = 3.0 \times 10^{-4}$, $V_r^G = 6.241$, $x_c^{LL} = 0.11241$, $V_r^{LL} = 1.386$) to C_2. The critical endpoints are shown in detail in figure 27.

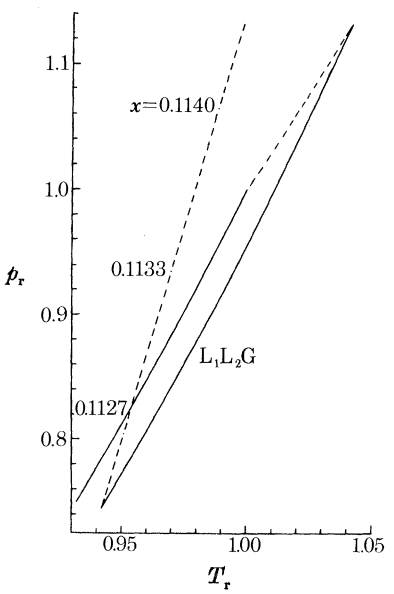

FIGURE 27. Enlargement of the region of the critical endpoints of the type-V system of figure 26 ($\zeta = 0.6, \Lambda = 0.0$).

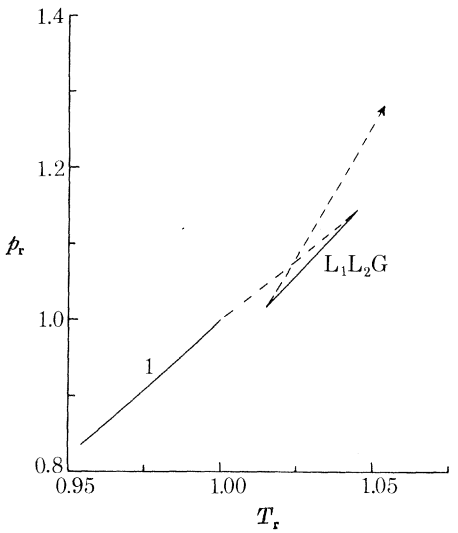

FIGURE 28. p_r, T_r-projection of a type-V phase diagram ($\zeta = 0.5833$, $\Lambda = 0.0833$). Enlargement of the region around the three-phase line. Both critical endpoints lie above C_1 (UCEP: $p_r = 1.146$, $T_r = 1.045$, $x_c^{GL} = 0.0074$, $V_r^{GL} = 2.531$, $x^L = 0.121$, $V_r^L = 1.434$; LCEP: $p_r = 1.015$, $T_r = 1.015$, $x^G = 0.0013$, $V_r^G = 3.95$, $x_c^{LL} = 0.058$, $V_r^{LL} = 1.604$).

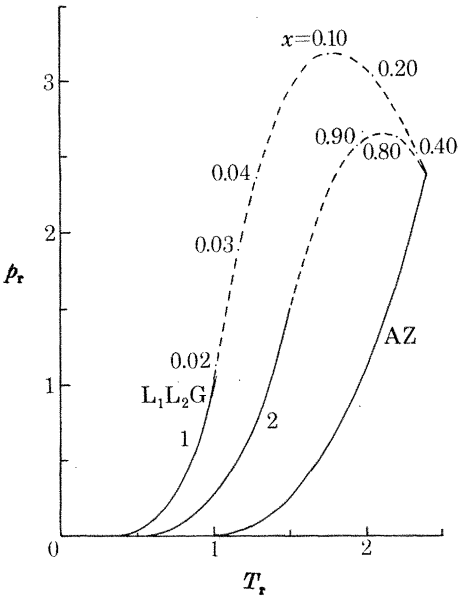

FIGURE 29. p_r, T_r-projection of a type-V-A phase diagram ($\zeta = 0.20$, $\Lambda = -1.80$). Two critical lines: C_1 to UCEP (G–L); LCEP to C_2 (L–L to G–L). One negative azeotrope line ($x^{AZ} = 0.556$). Details of the critical endpoints are shown in figure 30.

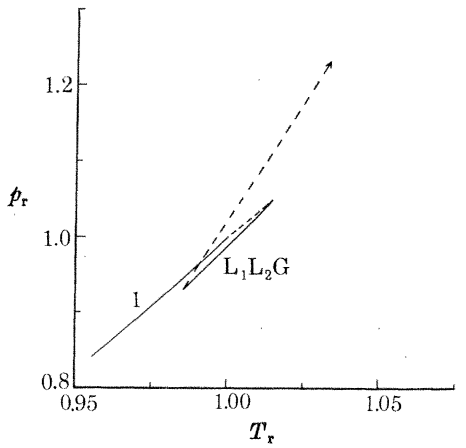

FIGURE 30. Enlargement of the region around the three-phase line for the p_r, T_r-projection of the type-V-A system of figure 29 ($\zeta = 0.20$, $\Lambda = -1.80$). (UCEP: $p_r = 1.051$, $T_r = 1.015$, $x^{GL} = 1.0 \times 10^{-3}$, $V_r^{GL} = 2.769$, $x^{L} = 0.0450$, $V_r^{L} = 1.555$; LCEP: $p_r = 0.928$, $T_r = 0.0985$, $x^{G} = 7 \times 10^{-5}$, $V_r^{G} = 4.3$, $x_c^{LL} = 0.0179$, $V_r^{LL} = 1.746$).

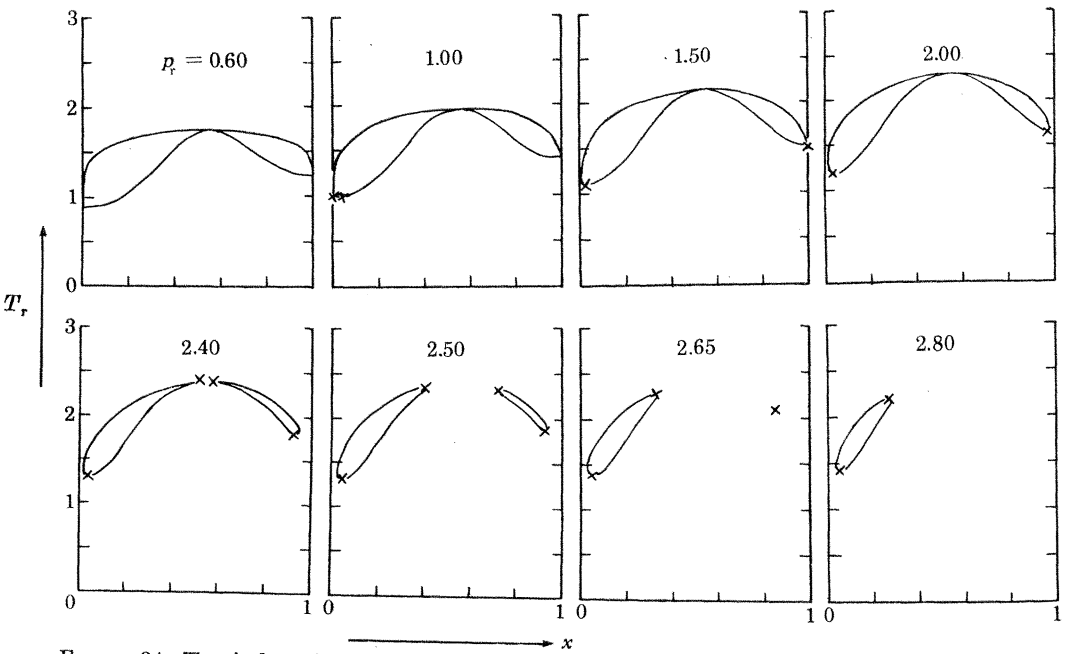

FIGURE 31. T_r, x-isobars for the type-V-A systems of figures 29 and 30 ($\zeta = 0.20$, $\Lambda = -1.80$).

Type V-A: the same as V, with the addition of a negative azeotrope

Finally, figures 29–31 show an example with an large negative value for Λ in region V-A that is unobtainable physically. Here negative azeotropy is combined with three-phase behaviour similar to that of region V. In all of the known experimental p, T-diagrams the first

maximum in the critical line near C_2 does not exist. This unusual feature means that the azeotropic T_r, x-diagrams divide into two branches before disappearing at higher pressures as shown in figures 31. Not all type-V-A diagrams show this behaviour; the azeotrope can also disappear as shown previously for an example in region I–A, figure 6. [The anomalous behaviour in figures 29–31 is not simply a result of the cusp in the critical line, which disappears when $\xi \neq 0$; even when $\xi \neq 0$ the smooth critical line can have two maxima when Λ is a large negative number.]

An experimental example is $H_2O + HCl$.

(*b*) *Symmetrical systems:* $\xi = 0, \zeta = 0$

When $\zeta = 0$ there are special solutions to the equation for the critical lines at $x = \frac{1}{2}$. The thermodynamic functions in this case are all symmetric about $x = \frac{1}{2}$. [The only real binary systems in which such symmetry occurs are mixtures of *d*, *l*-optical isomers (Scott 1977; liquid–liquid phase separation has not yet been reported for any such system, so the phase diagrams of this section are as yet hypothetical.]

It was shown in a foregoing section that the conditions for a critical point involved derivatives of the molar Helmholtz free energy A_m with respect to V_m and x. The imposed symmetry requires that all odd derivatives of A_m with respect to x must vanish at $x = \frac{1}{2}$:

$$A_x = A_{3x} = 0; \quad A_{xV} = A_{3xV} = 0; \quad A_{x2V} = A_{3x2V} = 0; \quad \text{etc.}$$

At any critical point

$$G_{2x} = A_{2x} - A_{xV}^2/A_{2V} = 0$$

and, since here $A_{xV} = 0$, this implies $A_{2x} = 0$. With the van der Waals equation, the solution of $A_{2x} = 0$ yields the only additional stable critical line for the symmetrical case:

$$p_r = T_r^2 \left[\frac{8}{T_m^\infty - T_r} - \frac{27}{(T_m^\infty)^2} + \frac{4}{T_m^\infty} \right], \tag{23}$$

where $T_m^\infty = \frac{27}{8}\Lambda$, as given by (14), when $\zeta = 0$.

When Λ is negative this critical line always remains at negative pressures and is certainly not a stable solution. When Λ is positive, part of this critical line becomes stable at high pressures.

The critical lines of phase diagrams along the Λ-axis are symmetric about $x = \frac{1}{2}$ and in the regions I-A and V-A (both have $\Lambda < 0$) they show the same features as when $\zeta > 0$. However the phase diagrams along the positive part of the Λ-axis differ in detail from those of regions II-A and III-HA on figure 1.

A phase diagram for $\zeta = 0$, situated adjacent to region III-HA, is shown in figure 32. The vapour-pressure curves 1 and 2 coincide and the critical line is symmetric about $x = \frac{1}{2}$. A three-phase line (L_1L_2G) extends from $p_r = T_r = 0$ and terminates at a UCEP (marked with a cross) at the beginning of a critical line at $x = \frac{1}{2}$, given by (23). Above the UCEP the $x = \frac{1}{2}$ critical line is stable and continues to infinite pressure. [This point, at which two critical lines intersect and a three-phase line ends is more than a UCEP; it is a *symmetrical tricritical point*. Unlike the usual unsymmetrical tricritical point, it could exist in a (symmetrical) binary system, and in principle one could observe experimentally three phases changing simultaneously to a single phase in a system of overall composition $x = \frac{1}{2}$. The low-pressure critical line has two branches ($x < \frac{1}{2}, x > \frac{1}{2}$) but these join smoothly on a T,x- or p,x-plot, intersecting the

$x = \frac{1}{2}$ critical line at right angles.] The series of T_r, x-diagrams in figure 33 shows how the gas–liquid critical points disappear smoothly so that only a single liquid–liquid critical point exists at high pressures, i.e. above the UCEP. [The phase diagrams are clearly just the symmetrical limit of type-III-HA diagrams, and the only new feature is the simultaneous disappearance (merging) of the gas–liquid critical points at the tricritical point.]

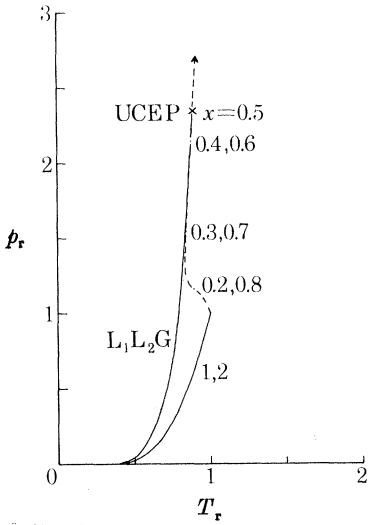

FIGURE 32. p_r, T_r-projection of the phase diagram of a symmetrical system ($\zeta = 0.0$, $\Lambda = 0.5$). The critical composition along the critical line above the UCEP is $x^c = \frac{1}{2}$. [The point labelled UCEP is in fact a symmetrical tricritical point; for explanation, see text.]

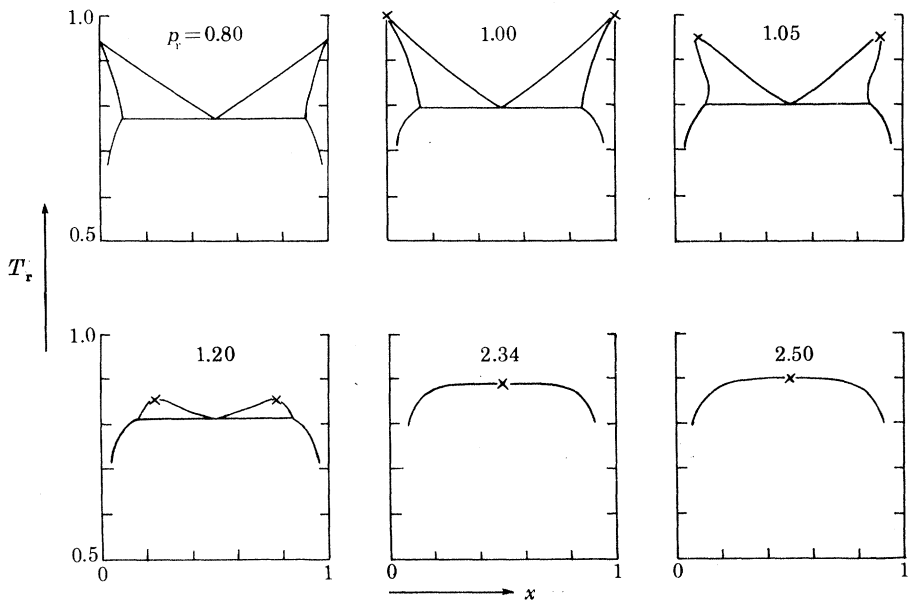

FIGURE 33. T_r, x-isobars for the symmetrical system of figure 32 ($\zeta = 0.0$, $\Lambda = 0.5$). [×, at $x = \frac{1}{2}$ on the T_r, x-diagram for $p_r = 2.34$, is the tricritical point.]

In figure 34 is shown an example with $\zeta = 0$, belonging to a region adjacent to region II-A. Here the gas–liquid critical line beginning at C_1 or C_2 ends at an azeotrope line at $x = \frac{1}{2}$. Another critical line begins at $p_r = 1.50$ when $x = \frac{1}{2}$ and is terminated just below the azeotrope line by a three-phase line. A second three-phase line beginning at $p_r = 1.5$ intersects

the first three-phase line and the azeotrope line at an unusual type of endpoint. A three-phase line then continues from this intersection to $p_r = T_r = 0$. Again the $x = \frac{1}{2}$ critical line becomes stable only at high pressures, in this example at $p_r = 1.5$, and continues to infinite pressure. [Here again, it is a tricritical point.]

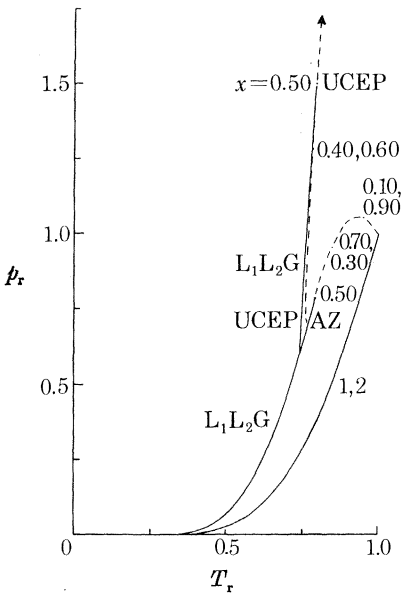

FIGURE 34. p_r, T_r-projection of a symmetrical system ($\zeta = 0.0$, $A = 0.42$). The critical composition along the critical line above the UCEP at high pressnre is $x^c = \frac{1}{2}$. [The UCEP at $x = 0.5$ is a symmetrical tricritical point; for explanation, see text.]

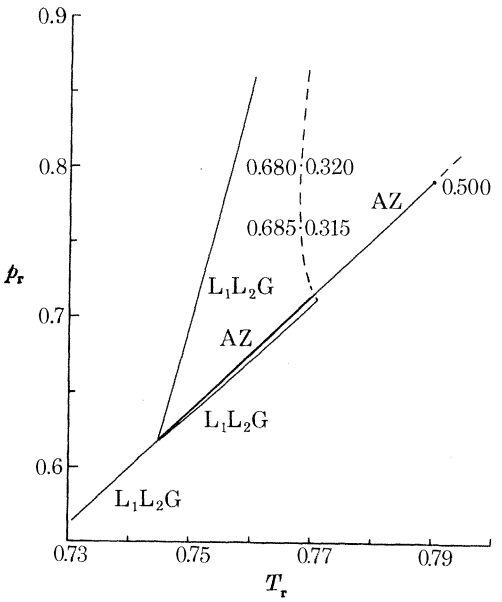

FIGURE 35. Enlargement of the region around the intersection of the azeotrope and the three-phase lines in the p_r, T_r-projection of the symmetrical phase diagram of figure 34 ($\zeta = 0.0$, $A = 0.42$). The two (mirror) UCEPs occur at $p_r = 0.715$, $T_r = 0.771$, and $x_c^{LL} = 0.311$, $x^G = 0.44$, or $x^G = 0.56$, $x_c^{LL} = 0.689$.

An enlargement of the region around the intersecting three-phase lines and azeotrope line is given in figure 35. At pressures such that $0.62 < p_r < 0.715$ the azeotrope and the three-phase lines lie so close together that even on this scale they would nearly coincide; therefore this three-phase line is purposely displaced to the right on the figure. A series of T_r, x-diagrams are given for this example in figure 36. At $p_r = 0.70$ and $p_r = 0.715$ no attempt is made to draw the azeotrope accurately. For these two pressures the region around $x = \frac{1}{2}$ is exaggerated in figure 37 to show the details more clearly.

[This phase diagram is clearly more complex than those for region II-A. In addition to the tricritical point, instead of one three-phase line there are three, and there is one extra pair of critical lines. All these features cannot disappear immediately when ζ ceases to be exactly zero, a fact that should have alerted us to the existence of the 'shield' region that Furman *et al.* (1977) found.]

[The 1968 dissertation overlooked two other kinds of phase diagrams along the $\zeta = 0$ line in the master diagram (figure 1) that were discovered by Furman & Griffiths (1978) and (in part independently) by Scott (1976, unpublished). The four types of symmetric phase diagrams can be summarized as follows.

(i) Symmetric II-A, $0 < \zeta < 0.3478$: a critical line, C_1 to C_2, with the upper end of an azeotrope line at its midpoint ($x = \frac{1}{2}$); a critical line at $x = \frac{1}{2}$, C_m to a UCEP, the upper end

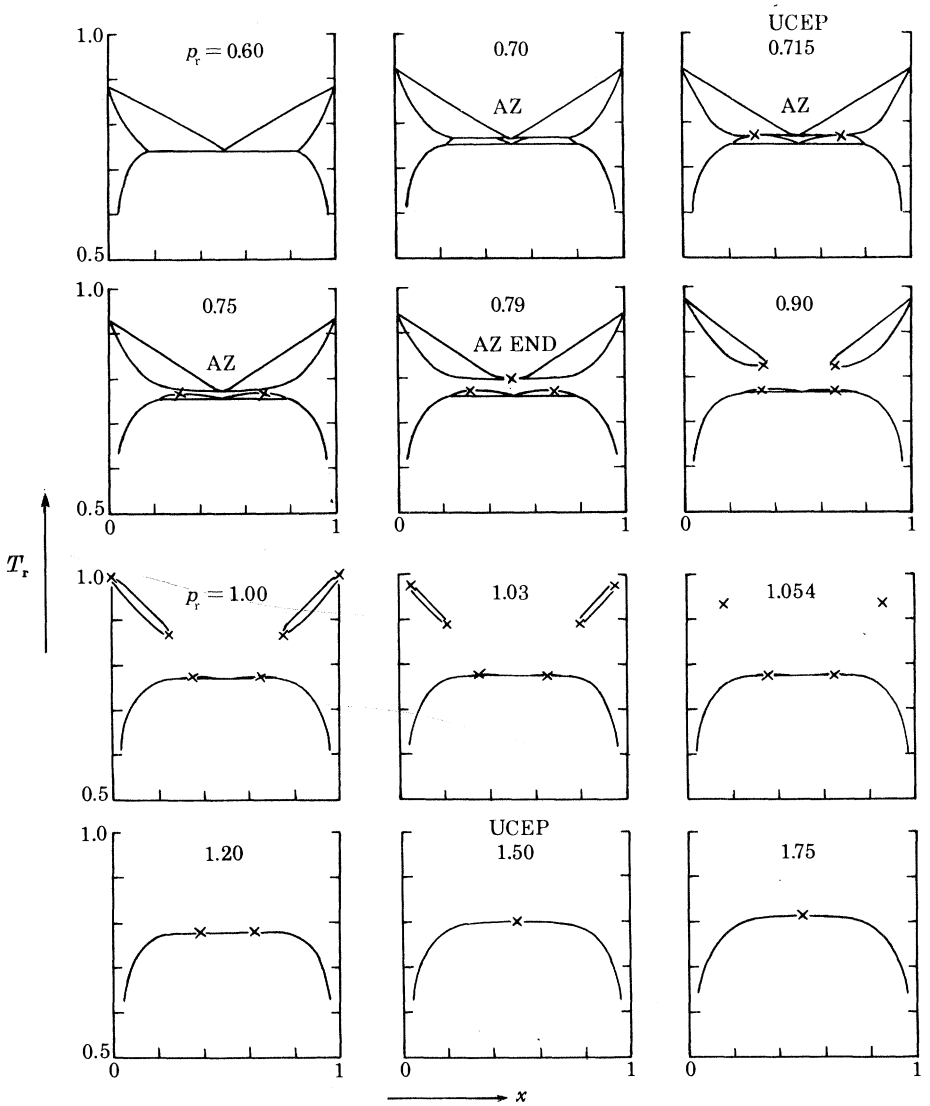

FIGURE 36. T_r, x-isobars for the symmetrical system of figures 34 and 35 ($\zeta = 0.0$, $\Lambda = 0.42$). The diagrams at $p_r = 0.70$ and $p_r = 0.715$ are schematically enlarged in figure 37. [The UCEP in the $p_r = 1.50$-diagram is a symmetrical tricritical point.]

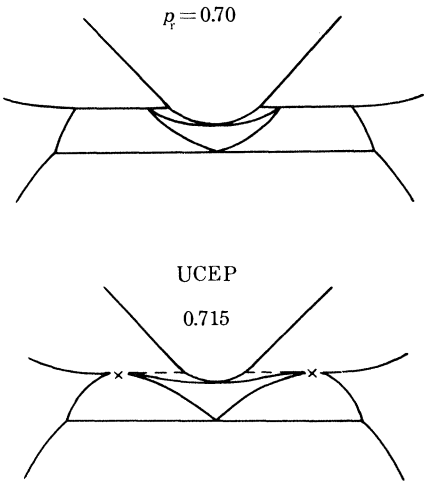

FIGURE 37. Schematic enlarged T_r, x-isobars for two pressures for the symmetrical system of figures 34–36 ($\zeta = 0.0$, $\Lambda = 0.42$).

of a three-phase line, which is also the lower end of the azeotrope line; no tricritical point. (Except for the symmetry this is similar to any other II-A diagram.)

(ii) Symmetric (II-A)*, $0.3478 < \zeta < 0.4364$ (see, for example, figures 34–36): a critical line, C_1 to C_2, with the upper end of an azeotrope line at its midpoint ($x = \frac{1}{2}$); a critical line at $x = \frac{1}{2}$, C_m to a tricritical point, which is also the UCEP for a three-phase line (α); a *third* critical line that runs from the central tricritical point to the UCEPs of separate three-phase lines (β' and β''), which at a lower temperature and pressure join the three-phase line α at the lower end of the azeotrope line to form a single three-phase line (γ).

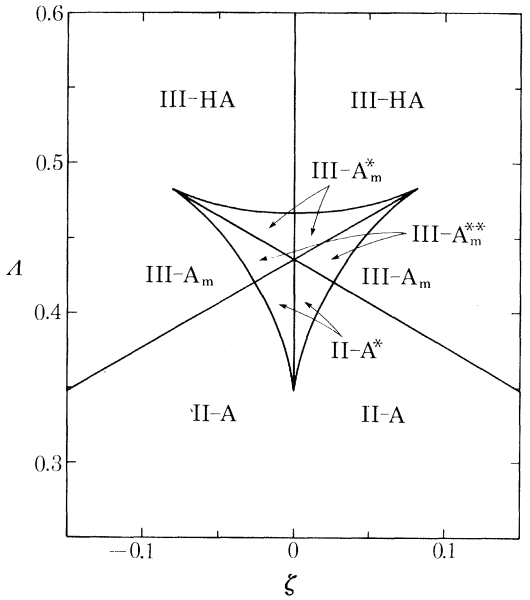

FIGURE 38. Enlargement of the main diagram (figure 1) in the region of $\zeta = 0.00$, $\Lambda = 0.43$ showing the 'shield' region and the regions representing special types II-A*, III-A_m^{**}, and III-A_m^*.

(iii) Symmetric (III-A)*, $0.4364 < \zeta < 0.4664$: a critical line, C_1 to C_2, each branch with a maximum and minimum pressure, with a tricritical point at $x = \frac{1}{2}$, which is also the UCEP for a three-phase line (α); a critical line at $x = \frac{1}{2}$, C_m to the tricritical point; a critical line that runs from the upper end of an azeotrope line ($x = \frac{1}{2}$) to the UCEPs of separate three-phase lines (β' and β''), which at a lower temperature and pressure join the three-phase line α at the lower end of the azeotrope line to form a single three-phase line (γ).

(iv) Symmetric III-HA (or III-HA_m), $0.4664 > \zeta$ (see, for example, figures 32–33): a critical line, C_1 to C_2, each branch with a maximum and minimum pressure for $\zeta \lesssim 0.493$, with a tricritical point at $x = \frac{1}{2}$, which is also the UCEP for a three-phase line; a critical line at $x = \frac{1}{2}$, C_m to the tricritical point; (except for the tricritical point generated by the symmetry, this is similar to other III-HA diagrams.)

[These especially complex diagrams of special symmetry lie along the midline of what Griffiths and co-workers have called the 'shield region', first discovered for a symmetrical three-component system by Furman *et al.* (1977) and later modified by Furman & Griffiths (1978) for a van der Waals binary mixture. The 'shield region' is shown on an enlarged Λ, ζ-plot in figure 38. (The boundaries are those calculated by Furman & Griffiths, converted to our units; the few calculations that we have made independently are in complete agreement with theirs.)]

[Figure 38 shows the shield region divided into six subregions by three lines of tricritical points, the symmetrical tricritical points at $\zeta = 0$ and two sets of tricritical points along the boundaries between type-II-A and -III-A_m behaviour. (The bands of type-IV* behaviour are too narrow to be shown). Away from the midline the phase diagrams are no longer completely symmetrical, but have the same complexity, as exemplified by three critical lines. In our terminology these can be classified as follows.

(i) Type (II-A)*: a critical line, C_1 to C_2, with the upper end of an azeotrope line joining it near $x = \frac{1}{2}$ (but at $x = \frac{1}{2}$ only if $\zeta = 0$); a critical line, C_m to a UCEP at the upper end of a three-phase line (β'); a third critical line connecting the UCEPs of separate three-phase lines (α and β''), which at a lower temperature and pressure join the three-phase line β' at the lower end of the azeotrope line to form a single three-phase line (γ).

(ii) Type (III-A)**: a critical line from C_m to C_2, with a minimum and a maximum in the p,x-curve; a critical line from C_1 to the upper end of an azeotrope line and on to a UCEP

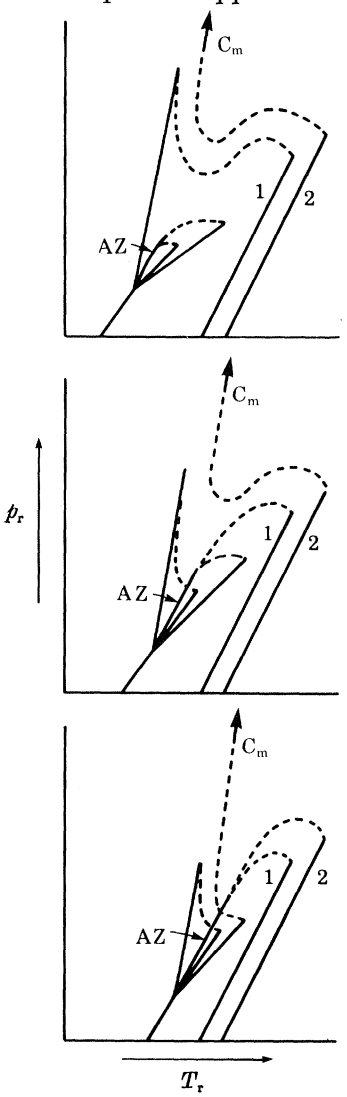

FIGURE 39. Schematic p_r,T_r-projections of phase diagrams for the special types II-A*, III-A_m^{**}, and III-A_m^*. The figures are not to scale, but are exaggerated for clarity. The unmarked solid lines are three-phase lines; in reality most of these will have slopes very nearly the same as those of the azeotrope and pure-liquid vapour-pressure curves, as in figures 34 and 35.

at the upper end of a three-phase line (β'); a third critical line connecting the UCEPs of separate three-phase lines (α and β''), which at a lower temperature and pressure join the three-phase line β' at the lower end of the azeotrope line to form a single three-phase line (γ).

(iii) Type (III-A)*: a critical line from C_m to C_2 with a minimum and a maximum in the p,x-curve; a critical line from C_1, with a minimum and a maximum in the p,x-curve, to a UCEP at the upper end of a three-phase line (α); a third critical line connecting the UCEPs of separate three-phase lines (β' and β''), with the upper end of an azeotrope line intermediate along the critical line; these two three-phase lines join the third (α) at the lower end of the azeotrope line to form a single three-phase line (γ). (For $\zeta < 0$, the roles of C_1 and C_2 are reversed.)

[Figure 39 shows schematic p,T-projections for these three special types, each drawn for ζ positive but close enough to zero that the relation to the symmetric diagrams should be self-evident. For systems close enough to $\zeta = 0$ all these must have real azeotropic behaviour; it is not certain, however, whether the III-A–III-HA and the III_m–III boundaries must necessarily lie outside the shield region.]

5. Phase diagrams for binary mixtures of molecules on unequal size

Van Konynenburg's (1968) dissertation (ch. IV) includes extensive calculations and figures for $\xi = \frac{1}{3}$ ($b_{22} = 2b_{11}$). Again the basic equation is (15) but now the volume parameter b varies linearly with the mole fraction (7). [For spherical molecules the more general quadratic dependence (6) (with the Lorentz expression for b_{12}) would doubtless be better, but most molecules are non-spherical. For linear molecules (for example, mixtures of n-alkanes), (7) is clearly preferable, but one perhaps should then replace the ideal mixing term in (10) by the analogous Flory formulation for polymers. (See, for example, Scott & van Konynenburg 1970). For modest differences in size, these different formulations all still lead to very similar phase diagrams.]

Here we merely summarize some of the general results and conclusions.

(i) No new major types of phase diagrams were discovered. The Λ,ζ master diagram for $\xi = \frac{1}{3}$ (figure 40) is no longer symmetrical around the $\zeta = 0$ axis, but the topological relations are essentially unchanged. For example, the II–IV boundary [i.e. the locus of unsymmetrical tricritical points] crosses the $\Lambda = 0$ axis at $\zeta = 0.28$ and $\zeta = -0.78$ rather than at $\zeta = \pm 0.56$ (for $\xi = 0$). There is a region of type-IV behaviour for a range of positive ζ's (0.26–0.30) along the geometric mean. The various regions of the diagram were not explored in nearly as much detail as they were for $\xi = 0$. [In particular it is not yet known whether a 'shield region' (like that shown in figure 38) occurs around the intersection of the three tricritical lines (now, all three, loci of unsymmetrical tricritical points).]

(ii) The azeotropic composition x^{AZ} is no longer independent of temperature and pressure. At very low temperature (i.e. at $T = 0$, ignoring the existence of solid phases) the azeotrope line starts at a mole fraction given by the equation

$$[\Lambda(1-\xi^2)+2\zeta\xi+2\xi^2]\,(\xi w-1)^2-\Lambda(1-\xi^2)^2 = 0, \tag{24}$$

where $w = 1-2x^{AZ}$. It can be shown that at most only one of the two roots of (24) corresponds to a value of x^{AZ} between 0 and 1. At low temperatures there can be at most one azeotrope

line, a result already known to van der Waals (1890). The limit of low-temperature azeotrope behaviour (i.e. when $x^{AZ} = 0$ or 1) is defined by two straight lines:

$$\Lambda(\xi \pm 1) = \xi + \zeta, \tag{25}$$

which are shown in figure 40.

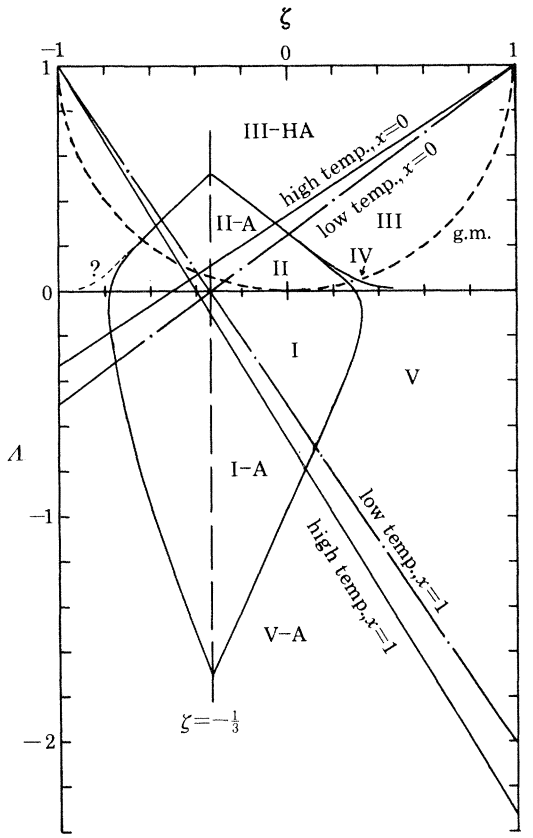

FIGURE 40. Diagram of phase behaviour for molecules of unequal size ($\xi = \frac{1}{3}$).

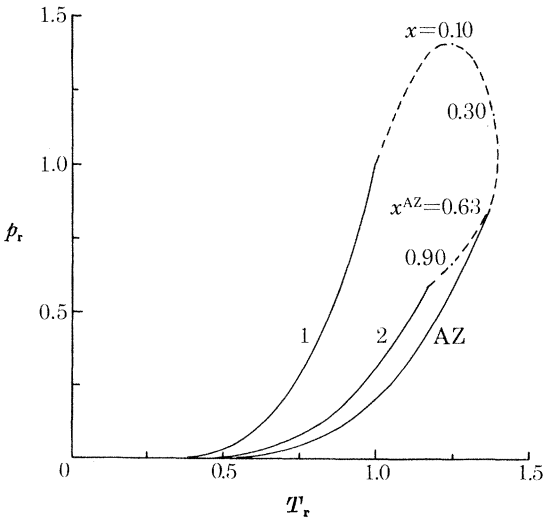

FIGURE 41. p_r, T_r-projection of a type I–A phase diagram ($\zeta = -0.263$, $\Lambda = -0.579$, $\xi = \frac{1}{3}$).

The azeotrope line ends at high temperature by joining a critical line at a mole fraction given by the equation

$$2[\Lambda(1-\xi^2)+2\zeta\xi+2\xi^2]\ (\xi w-1)^2+\Lambda(1-\xi^2)\ (\xi w-2+\xi^2)+\zeta\xi(1-\xi^2)\ (\xi w-1)\ =\ 0. \quad (26)$$

The junction is now tangential as is shown in figure 41. The unusual cusp in the critical line, found when $\xi = 0$, has disappeared. The limit of high-temperature azeotrope behaviour ($x^{AZ} = 0$ or 1) is defined by two more straight lines:

$$3\Lambda(\xi \pm 1)\ =\ 4\xi+\zeta(3\mp\xi). \quad (27)$$

For $\xi \neq 0$, this pair of lines is displaced from the low-temperature lines and, for any system lying in the narrow sector of Λ,ζ-space between the two lines, the azeotrope line appears or disappears at $x = 0$ or $x = 1$ at an intermediate temperature.

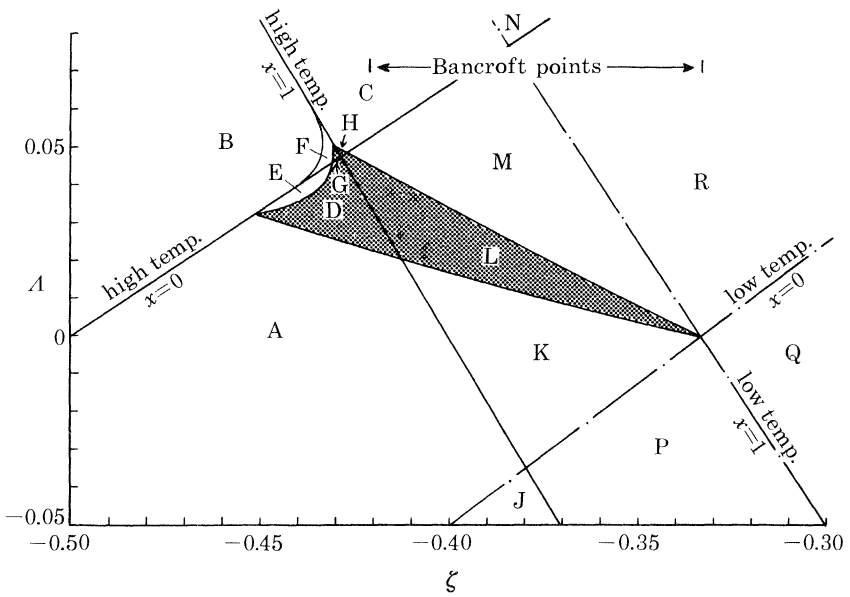

FIGURE 42. Enlargement of the region of double azrotropy (shaded) for $\xi = \frac{1}{3}$. The regions A to R correspond to the T,x-projections in figure 43. For an explanation of Bancroft points see text.

Azeotropy is very likely to be found experimentally in systems where the vapour pressures of the two pure components are very similar. In some systems the vapour-pressure curves actually cross on the p,T-projection; the intersection is called a *Bancroft point*. Except for an ideal mixture, the existence of a Bancroft point always implies azeotropy, but none of the classes of azeotrope lines require the existence of a Bancroft point. For $\xi = 0$ the vapour-pressure curves do not cross; for $\xi = \frac{1}{3}$ Bancroft points are produced with the van der Waals equation for values of ζ between $-\frac{1}{3} = -0.333$ and -0.423.

(iii) A very special feature of a small region of Λ,ζ-space for $\xi = \frac{1}{3}$ was the discovery of systems with double azeotropes, i.e. with both minimum and maximum boiling mixtures in the same phase diagram. Figure 42 shows au enlargement of the Λ,ζ-master diagram in this region. The shaded region is where the double azeotropes occur. The letters A–R designate different kinds of T,x-projections of the critical and azeotrope lines that are shown schematically

in figure 43. All the double azeotrope systems arise from a single azeotrope line that has a minimum in the T,x-projection, i.e. the two extrema coalesce at a lower temperature. There is no evidence to suggest that the first system for which there is unambiguous experimental evidence of double azeotropy, benzene + hexafluorobenzene studied by Gaw & Swinton (1966; 1968), has this property.

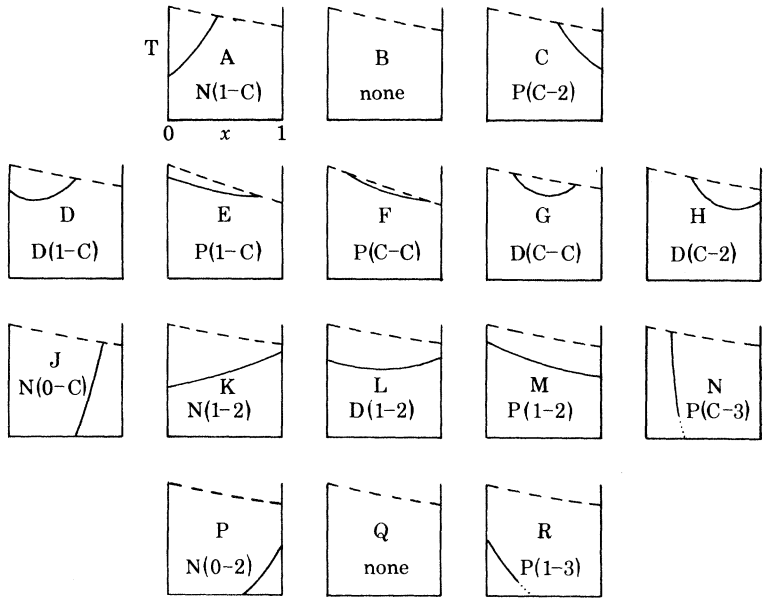

FIGURE 43. Schematic T_r,x-projections for the fourteen possible types of azeotrope lines for $\xi \neq 0$. The labels A to R refer to the regions in figure 42. N(1–C): negative azeotrope line running from the vapour-pressure curve of pure liquid 1 to the critical line; P(C–3): positive azeotrope line starting at the critical line and ending on a three-phase line; D(C–C): double azeotrope line starting and ending on the critical line; etc.

The authors wish to thank R. B. Griffiths, C. M. Knobler, I. A. McLure, J. S. Rowlinson, J. C. Wheeler and A. G. Williamson for many helpful discussions and useful suggestions. The research of which this is a part is supported by the U.S. National Science Foundation.

APPENDIX A. CALCULATION OF CRITICAL LINES AND PHASE DIAGRAMS FOR A VAN DER WAALS BINARY MIXTURE WITH $\xi = 0$

Equations (16) and (17) were solved simultaneously by using (15) for the Helmholtz free energy. After much lengthy algebra an equation, $F = 0$, which is seventh order in both V_r and x was obtained (here, V is written for $V_r = V_m/b$).

$$\begin{aligned} F \equiv\ & V^6(V-3)\gamma^3z^3w + 3V^4(V-1)^2(V-3)\beta\gamma^2z^3 \\ & - 6V^4(V-1)^2\gamma[\alpha\gamma(V-3) - \beta^2(V-2)]z^2w \\ & - V^4(V-1)^3\beta^3zw^2 - 4V^2(V-1)^3\beta[3\alpha\gamma(V-1)(V-3) \\ & - \beta^2(2V-3)^2]z^2 + 12V^2(V-1)^4\alpha[\alpha\gamma(V-3) - \beta^2(V-2)]zw \\ & + 12(V-1)^6(V-3)\alpha^2\beta z - 8(V-1)^6(V-3)\alpha^3w = 0, \end{aligned} \tag{A 1}$$

where $z = x(1-x)$, $w = \mathrm{d}z/\mathrm{d}x = 1-2x$,

$$\alpha = \frac{a_m}{a_{11}} = (1-x)^2 + 2x(1-x)\left(\frac{a_{12}}{a_{11}}\right) + x^2\left(\frac{a_{22}}{a_{11}}\right)$$
$$= (1-w\zeta-2z\Lambda)/(1-\zeta),$$

$$\beta = \frac{\mathrm{d}\alpha}{\mathrm{d}x} = 2\left(\frac{a_{12}}{a_{11}}-1\right) + 2\left(1+\frac{a_{22}}{a_{11}}-\frac{2a_{12}}{a_{11}}\right)x$$
$$= 2(\zeta-w\Lambda)/(1-\zeta),$$

and

$$\gamma = \frac{\mathrm{d}^2\alpha}{\mathrm{d}x^2} = 2\left(1+\frac{a_{22}}{a_{11}}-2\frac{a_{12}}{a_{11}}\right)$$
$$= 4\Lambda/(1-\zeta).$$

The auxiliary expressions for the reduced temperature and pressure are

$$T_r = \frac{\frac{27}{8}[2\alpha\beta w(V-1)^3 + 2\alpha\gamma z(V-1)^2(V-3) - 2\beta^2 z(V-1)^2(2V-3) - \gamma^2 z^2 V^2(V-3)]}{2\alpha V(V-1)^2(V-3) + \beta w V^3(V-1) - \gamma z V^3(V-3)}, \tag{A 2}$$

$$p_r = \frac{8T_r}{V-1} - \frac{27\alpha}{V^2}. \tag{A 3}$$

Roots (values of V_r) were obtained for fixed values of Λ, ζ and x. The computer program first examined the sign of F at $V_r = 1+\Delta V_r$, where, typically, ΔV_r was chosen as 0.05. The sign of F was examined again for successive additions of ΔV_r to V_r until F changed sign. This located the root between the current value of V_r and $V_r - \Delta V_r$. ΔV_r was replaced by half of its original value and the sign of F was examined for $V_r' = V_r - \Delta V_r$. This process was repeated for a fixed number of iterations (usually 5–10 depending on the accuracy desired). A mean value of V_r (called V_{mid}) was computed from the last immediately preceding values of V_r, V_{high} and V_{low}, and of F, $F(V_{high})$ and $F(V_{low})$.

$$V_{mid} = \frac{F(V_{high})\,V_{low} - F(V_{low})\,V_{high}}{F(V_{high}) - F(V_{low})}.$$

The corresponding values of T_r and p_r were also calculated and printed in the output.

After one root had been found, another root was obtained by repeating the process with a starting value of V_r equal to the previous root plus ΔV_r. Apparently, when $V_r = 3$ the range of meaningful roots was exhausted (there were never any unaccountable endpoints to critical lines). The entire process was then repeated by starting with a new value of x, and $V_r = 1+\Delta V_r$. The program continued until all the selected values of x had been examined. The work was done on the U.C.L.A. IBM model 7094 and model 360-75 computers. Physically meaningless roots corresponding to negative temperatures were always discarded; roots corresponding to negative pressure are at best metastable but were not automatically discarded.

The procedures necessary to obtain the stable coexistent phases of a two-component system are very similar to the well known ones used for the one-component system. For a two-component system the relative activities λ_1^* and λ_2^* of components 1 and 2 are defined by the equations

$$\ln \lambda_1^* = [\mu_1 - \mu_{i,1}^{\ominus}(V_m^{\ominus})]/RT, \tag{A 4a}$$

$$\ln \lambda_2^* = [\mu_2 - \mu_{i,2}^{\ominus}(V_m^{\ominus})]/RT. \tag{A 4b}$$

In terms of reduced parameters the activities for $\xi = 0$ ($b_{11} = b_{22} = b$), after setting $V_m^{\ominus} = b$, become

$$\ln \lambda_1^* = -\frac{27[1-x+x(a_{12}/a_{11})]}{4T_r V_r} + \ln\left(\frac{1-x}{V_r-1}\right) + \frac{1}{V_r-1}, \tag{A 5a}$$

$$\ln \lambda_2^* = -\frac{27[(1-x)\,(a_{12}/a_{11})+x(a_{22}/a_{11})]}{4T_r V_r} + \ln\left(\frac{x}{V_r-1}\right) + \frac{1}{V_r-1}. \tag{A 5b}$$

For a mixture at constant temperature and pressure the appropriate free-energy plot is the molar Gibbs free energy G_m against x. A computer program was designed to solve the van der Waals equation for x at constant p_r and T_r for a series of values of V_r. The values of V_r, T_r and x were in turn used in (A 5a) and (A 5b) to calculate a series of activities. The activities were used to calculate a free energy function

$$(G_m - G_m^{\ominus})/RT = (1-x)\ln \lambda_1^* + x \ln \lambda_2^*, \tag{A 6}$$

which was then plotted against x by a Calcomp model 765 plotter.

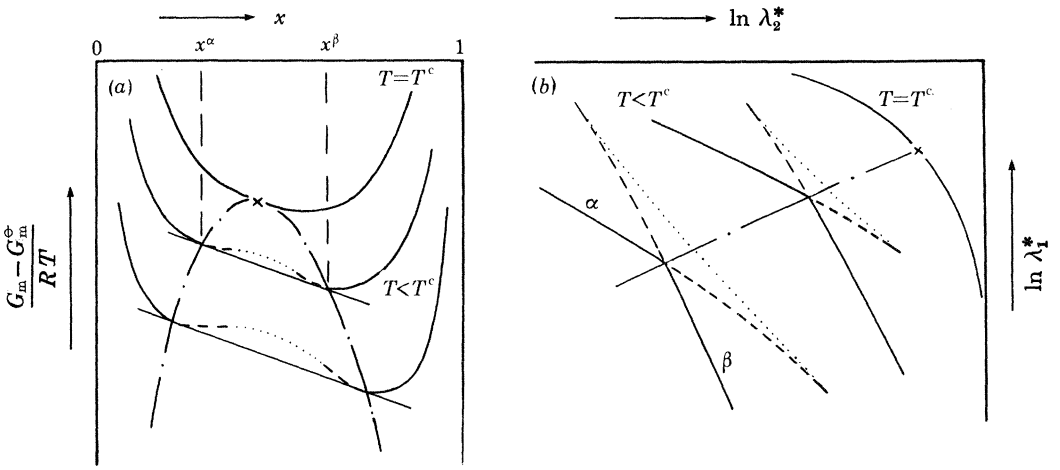

FIGURE A 1. Three isotherms of a binary mixture near a UCST (the same constant pressure for all three). (*a*) Gibbs free energy, G (divided by RT), against mole fraction x; (*b*) $\ln \lambda_1$, the activity of component 1 against $\ln \lambda_2$ the activity of component 2.

The form of the curves produced is shown schematically for three isotherms in figure A 1*a* for a system going from a two-phase to a one-phase system with increasing temperature at constant pressure. For values of the free energy and composition along the dashed (metastable) or dotted (unstable) portions of the curve, the system can have lower free energy by dividing into two phases the compositions of which are determined by the points where a straight line meets the curve at a tangent. At the critical point the two coexistent phases become identical and the metastable and unstable portions of the curve disappear at a point (marked with a cross).

The corresponding activity plot is given in figure A 1*b* for the three isotherms shown in figure A 1*a*. Two phases, α and β, coexist when

$$\mu_1^\alpha = \mu_1^\beta, \quad \mu_2^\alpha = \mu_2^\beta \quad (\text{constant } T,p),$$

that is, at the intersection of the two stable branch curves. Like the tangent line in figure A 1*a*, the intersection on the activity plot defines a point on the coexistence curve (—·—). A computer program was used to calculate these points of intersection and the results were used to construct T_r, x-phase diagrams at constant pressure for the mixtures described earlier.

By definition a UCEP occurs in fluid systems when a three-phase line (L_1L_2G) intersects a critical line as the temperature is increased. Suppose the situation is as shown in the p_r, T_r-diagram in figure A 2*a*, a typical case of limited miscibility close to the gas–liquid critical point of the volatile component. The full lines represent the vapour-pressure curve of component 1 (labelled 1), and the three-phase line (labelled L_1L_2G). The vapour-pressure curve of component 2 is not shown. (For an example of a typical complete diagram, see figure 26.) Typical calculated critical lines are shown as dashed lines.

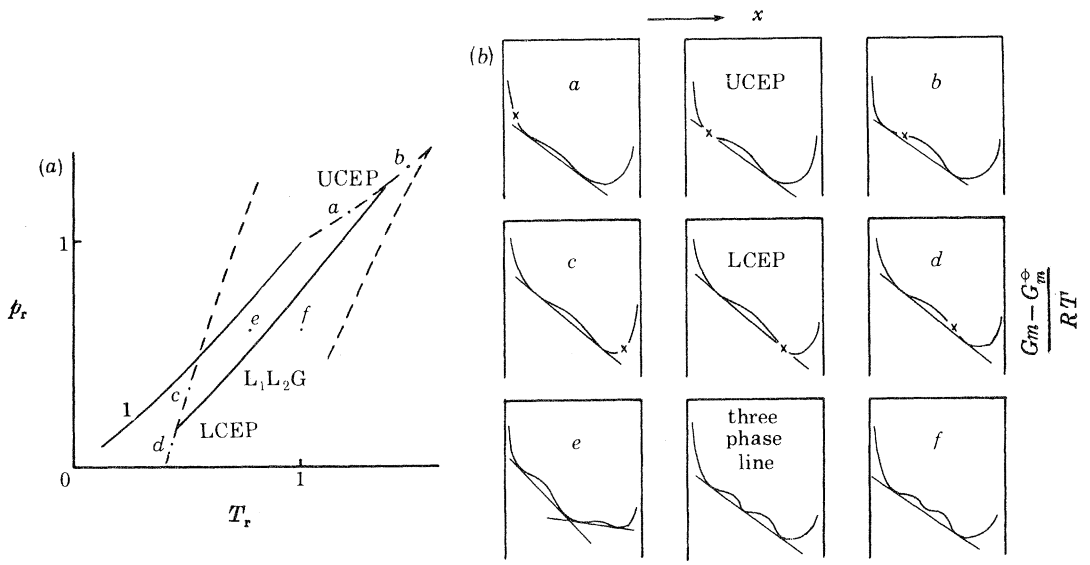

FIGURE A 2. (*a*) Enlargement of a high-temperature three-phase line bounded by a UCEP and a LCEP. (*b*) Gibbs free energy against mole fraction at the points on the phase diagram in (*a*).

In the plots of $(G_m - G^{\ominus}_m)/RT$ against x in figure A 2*b*, the curves *a*–*d* are for different values of x^c (each having different values of p_r and T_r) and correspond to the critical points *a*–*d* shown in figure A 2*a*. (The metastable and unstable portions of the curves are not shown as dashed and dotted lines as earlier.) For the point *a*, the critical point on the G, x-curve (marked with a cross ×) lies at a low mole fraction outside the two-phase part of the curve. At the UCEP, a second (liquid) phase with a larger value of x than the critical composition is in equilibrium with the critical mixture. Point *b* is typical of points belonging to a metastable portion of the critical line.

A LCEP occurs when a three-phase (L_1L_2G) line intersects a critical line as the temperature is lowered. Along the critical line above the LCEP a critical point such as *c* lies outside the two-phase portion of the G, x-curve. At the LCEP a gaseous phase is in equilibrium with the critical (liquid) mixture. The point *d* lies on a metastable part of the critical line.

The points *e* and *f* in figure A 2 correspond to values of p_r and T_r where more than one phase is stable. Point *e* lies between the vapour-pressure curve (1) and the three-phase line. At this value of p_r and T_r there are two equilibria: $G(x') - L(x'')$ and $L(x''') - L(x^{(iv)})$. At the three-phase line two liquid phases and a gas phase $[G(x') - L(x'') - L(x^{(iv)})]$ are in equilibrium and at point *f* only two phases $[G(x') - L(x^{(iv)})]$ are stable.

In figure A 3 activity plots of $\ln \lambda_1^*$ against $\ln \lambda_2^*$ are given for the points *a*–*f* in figure A 2. (The metastable and unstable portions of the curve are not shown as dashed and dotted lines.)

The critical point (a) lies along the gaseous branch (G) outside the area enclosed by the intersecting branches; the UCEP is reached when the liquid branch (L) intersects the gaseous branch at the critical point; the point b lies on a metastable part of the critical line. Point c lies outside the area enclosed by the liquid and gaseous branches; at the LCEP the gaseous branch intersects the liquid branch at the critical point; point f lies on a metastable part of the critical line.

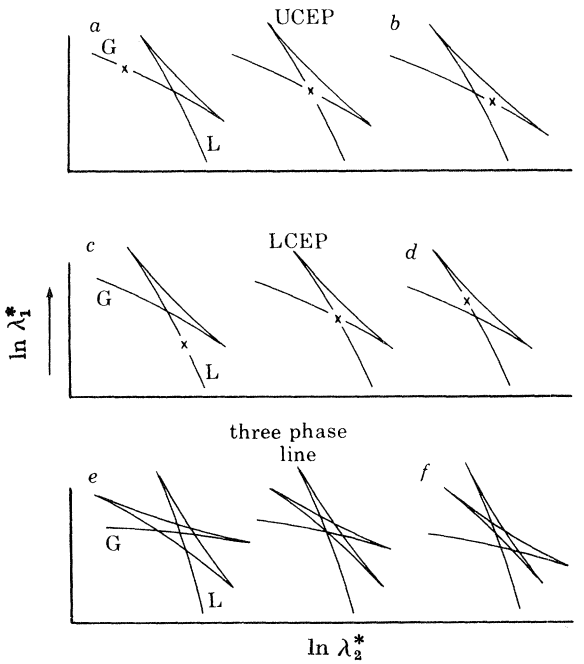

FIGURE A 3. $\ln \lambda_1^*$, the logarithm of the activity of component 1, against $\ln \lambda_2^*$, the logarithm of the activity of component 2, at the points on the phase diagram in figure A 2a.

A three-phase line that intersects a low-temperature liquid–liquid UCST line is analysed in the same manner as the high-temperature UCST.

A computer program was designed to find critical endpoints along critical lines by calculating the intersections of branch lines of activity plots at critical points (see figure A 3). Some of the results were given with the calculated phase diagrams of § 4.

Points along three-phase lines were found in the following way. For a fixed value of p_r and T_r a series of values of V_r was used to calculate a set of compositions by solving the van der Waals equation for x. These values of V_r and x, along with p_r and T_r, were used in (A 5a) and (A 5b) to calculate $\ln \lambda_1^*$ and $\ln \lambda_2^*$. A series of plots similar to the three phase line plots shown in figure A 3 were made at a fixed value of p_r to find the value of T_r at which the three stable branches intersected at the same point.

APPENDIX B. THE VAPOUR PRESSURE OF A PURE VAN DER WAALS FLUID

A computer program was designed to calculate the reduced pressure (p_r), temperature (T_r) and coexisting volumes of gas (V_r^G) and liquid (V_r^L) along the vapour-pressure curve of a one-component van der Waals fluid. This was accomplished by plotting p_r against $\ln \lambda$ in a

way entirely analogous to the ln λ_1^* against ln λ_2^* plots of Appendix A. By applying the condition $(\partial p/\partial V)_T = 0$ to the van der Waals equation (2) for a particular value of T_r, two roots (values of V_r) are found. The larger value of V_r was used in the program to calculate the pressure maximum (where the metastable gas ends and the mechanically unstable fluid begins). While the same value of T_r was retained, p_r was decreased by decrements Δp_r. At each new pressure there are three roots to the van der Waals equation corresponding to the volumes of the liquid, the metastable gas and the mechanically unstable fluid. The volumes of the liquid and the metastable gas phases are the smallest and largest respectively of the three roots and were used to calculate ln λ^L and ln λ^G from (A 5a) with $x = 0$. The pressure was decreased by decrements Δp_r until the difference ln $\lambda^L - \ln \lambda^G$ changed sign. The sign of ln $\lambda^L - \ln \lambda^G$ was then examined at $p_r' = p_r + \frac{1}{2}\Delta p_r$ and so on until $\Delta p_r/p_r < 5 \times 10^{-5}$. The values of p_r, V_r^L, V_r^G, ln λ^L and ln λ^G were all printed out at each new value of p_r for each isotherm so that convergency could be checked. The resulting values of T_r, p_r, V_r^L and V_r^G are given in table 1. The last six entries at low pressure were recalculated with more significant figures than were used for the rest of the table to improve convergence. The densities (inverse volumes) of the coexisting phases and the 'diameter' (average density) of the coexistence curve are also tabulated.

TABLE 1. VAPOUR–LIQUID EQUILIBRIA FOR A PURE VAN DER WAALS FLUID

T_r	p_r	$V_r^L = V_m^L/b$	$V_r^G = V_m^G/b$	$\rho^L = 1/V_r^L$	$\rho^G = 1/V_r^G$	$\frac{1}{2}(\rho^L+\rho^L)$
1.00000	1.00000	3.0000	3.0000	0.33333	0.33333	0.33333
0.99000	0.96047	2.4928	3.7291	0.40116	0.26816	0.33466
0.98000	0.92191	2.3266	4.1283	0.42981	0.24223	0.33602
0.97000	0.88430	2.2127	4.4880	0.45194	0.22282	0.33738
0.96000	0.84761	2.1246	4.8356	0.47068	0.20680	0.33874
0.95000	0.81187	2.0524	5.1814	0.48723	0.19300	0.34012
0.94000	0.77707	1.9911	5.5315	0.50223	0.18078	0.34151
0.93000	0.74317	1.9378	5.8905	0.51605	1.16976	0.34291
0.92000	0.71021	1.8907	6.2607	0.52890	0.15973	0.34432
0.91000	0.67814	1.8485	6.6456	0.54098	0.15048	0.34573
0.90000	0.64699	1.8102	7.0467	0.55242	0.14191	0.34717
0.89000	0.61673	1.7753	7.4669	0.56328	0.13392	0.34860
0.88000	0.58736	1.7432	7.9081	0.57366	0.12645	0.35006
0.87000	0.55887	1.7135	8.3728	0.58360	0.11943	0.35152
0.86000	0.53125	1.6859	8.8635	0.59315	0.11282	0.35299
0.85000	0.50449	1.6601	9.3829	0.60237	0.10658	0.35448
0.84000	0.47858	1.6359	9.9342	0.61128	0.10066	0.35597
0.83000	0.45353	1.6132	10.5192	0.61988	0.09506	0.35747
0.82000	0.42931	1.5918	11.1426	0.62822	0.08974	0.35898
0.81000	0.40592	1.5715	11.8073	0.63633	0.08469	0.36051
0.80000	0.38335	1.5522	12.5177	0.64425	0.07989	0.36207
0.79000	0.36159	1.5340	13.2782	0.65189	0.07531	0.36360
0.78000	0.34064	1.5166	14.0935	0.65937	0.07095	0.36516
0.77000	0.32046	1.5000	14.9704	0.66667	0.06680	0.36673
0.76000	0.30107	1.4841	15.9129	0.67381	0.06284	0.36833
0.75000	0.28246	1.4689	16.9288	0.68078	0.05907	0.36993
0.74000	0.26458	1.4543	18.029	0.68762	0.05547	0.37154
0.73000	0.24746	1.4404	19.217	0.69425	0.05204	0.37314
0.72000	0.23106	1.4270	20.508	0.70077	0.04876	0.37477
0.71000	0.21541	1.4140	21.909	0.70721	0.04564	0.37643
0.70000	0.20044	1.4016	23.436	0.71347	0.04267	0.37807
0.69000	0.18617	1.3896	25.103	0.71963	0.03984	0.37973
0.68000	0.17260	1.3780	26.923	0.72569	0.03714	0.38142
0.67000	0.15970	1.3668	28.919	0.73164	0.03458	0.38311
0.66000	0.14741	1.3560	31.122	0.73746	0.03213	0.38480

PHILOSOPHICAL TRANSACTIONS OF THE ROYAL SOCIETY A MATHEMATICAL, PHYSICAL & ENGINEERING SCIENCES

TABLE 1 (*cont.*)

T_r	p_r	$V_r^L = V_m^L/b$	$V_r^G = V_m^G/b$	$\rho^L = 1/V_r^L$	$\rho^G = 1/V_r^G$	$\frac{1}{2}(\rho^L+\rho^L)$
0.65000	0.13580	1.3456	33.541	0.74316	0.02981	0.38649
0.64000	0.12481	1.3354	36.213	0.74884	0.02761	0.38823
0.63000	0.11445	1.3256	39.168	0.75438	0.02553	0.38995
0.62000	0.10468	1.3161	42.446	0.75982	0.02356	0.39169
0.61000	0.09547	1.3069	46.114	0.76517	0.02168	0.39343
0.60000	0.08683	1.2979	50.213	0.77048	0.01992	0.39520
0.59000	0.07875	1.2892	54.797	0.77567	0.01825	0.39696
0.58000	0.07115	1.2807	59.991	0.78082	0.01667	0.39875
0.57000	0.06411	1.2725	65.831	0.78585	0.01519	0.40052
0.56000	0.05751	1.2645	72.50	0.79083	0.01379	0.40231
0.55000	0.051580	1.2565	79.83	0.79586	0.01253	0.40419
0.50000	0.027788	1.2203	137.95	0.81947	0.00725	0.41336
0.45000	0.013134	1.1881	267.44	0.84168	0.00374	0.42271
0.40000	0.0051761	1.1592	610.69	0.86266	0.00164	0.43215
0.35000	0.0015747	1.1331	1769.4	0.88253	0.00056	0.44155
0.30000	0.0003525	1.1081	6798	0.90244	0.00015	0.45130

REFERENCES

Clancy, P., Gubbins, K. E. & Gray, C. G. 1978 *Discuss. Faraday Soc.* **66**, 116.
Creek, J. L., Knobler, C. M. & Scott, R. L. 1977 *J. chem. Phys.* **67**, 366.
Davenport, A. J. & Rowlinson, J. S. 1963 *Trans. Faraday Soc.* **59**, 78.
Davenport, A. J., Rowlinson, J. S. & Saville, G. 1966 *Trans. Faraday Soc.* **62**, 322.
Dickinson, E., Knobler, C. M. & Scott, R. L. 1973 *J. chem. Soc. Faraday Trans.* I **69**, 2179.
Freeman, P. I. & Rowlinson, J. S. 1960 *Polymer* **1**, 20.
Furman, D., Dattagupta, S. & Griffiths, R. B. 1977 *Phys. Rev.* B **15**, 441.
Furman, D. & Griffiths, R. B. 1978 *Phys. Rev.* A **17**, 1139.
Gaw, W. J. & Swinton, F. L. 1966 *Nature, Lond.* **212**, 283.
Gaw, W. J. & Swinton, F. L. 1968 *Trans. Faraday Soc.* **64**, 2023.
Griffiths, R. B. 1974 *J. chem. Phys.* **60**, 195.
Guggenheim, E. A. 1952 *Mixtures*. London: Oxford University Press.
Hicks, C. P. & Young, C. L. 1971 *Trans. Faraday Soc.* **67**, 1598.
Hicks, C. P. & Young, C. L. 1975 *Chem. Rev.* **75**, 119.
Hicks, C. P. & Young, C. L. 1977 *J. chem. Soc. Faraday Trans.* II **73**, 597.
Hildebrand, J. H. & Wood, S. E. 1933 *J. chem. Phys.* **1**, 817.
Hurle, R. F., Jones, F. & Young, C. L. 1977 *J. chem. Soc. Faraday Trans.* II **73**, 613.
Kamerlingh Onnes, H. *et al.* 1900 *Commun. Lab. Univ. Leiden.* nos 59*a*, 59*b*, 64.
Kamerlingh Onnes, H. *et al.* 1901 *Commun. Lab. Univ. Leiden.* nos 65, 75, suppl. no. 5.
Kamerlingh Onnes, H. *et al.* 1902 *Commun. Lab. Univ. Leiden.* nos 79, 81, suppl. no. 6.
Kamerlingh Onnes, H. *et al.* 1903 *Commun. Lab. Univ. Leiden.* suppl. no. 7.
Kamerlingh Onnes, H. *et al.* 1904 *Commun. Lab. Univ. Leiden.* suppl. no. 8.
Kamerlingh Onnes, H. *et al.* 1906 *Commun. Lab. Univ. Leiden.* nos 96*a–c*, suppl. no. 11.
Kamerlingh Onnes, H. *et al.* 1907 *Commun. Lab. Univ. Leiden.* suppl. nos 14–16.
McGlashan, M. L., Stead, K. & Warr, C. 1973 Third International Conference on Chemical Thermodynamics (Baden, Austria): preprints, vol. II, p. 228.
McGlashan, M. L., Stead, K. & Warr, C. 1977 *J. chem. Soc. Faraday Trans.* II **73**, 1889.
McKinnon, I. R. 1967 Ph.D. thesis, University of Exeter.
Marsh, K. N., McGlashan, M. L. & Warr, C. 1970 *Trans. Faraday Soc.* **66**, 2453.
Rowlinson, J. S. 1959 *Liquids and liquid mixtures*. London: Butterworths.
Rowlinson, J. S. 1969 *Liquids and liquid mixtures* (2nd edn). London: Butterworths.
Rowlinson, J. S. 1970 *Discuss. Faraday Soc.* **49**, 30.
Rowlinson, J. S. & Freeman, P. I. 1961 *Pure appl. Chem.* **2**, 329.
Scatchard, G. 1931 *Chem. Rev.* **8**, 321.
Schneider, G. 1966 *Ber. BunsenGes. phys. Chem.* **70**, 497.
Schneider, G. 1970 *Fortschr. chem. Forsch.* **13**, 559.
Scott, R. L. 1970 *Discuss. Faraday Soc.* **49**, 76.
Scott, R. L. 1971 *Ber. BunsenGes. phys. Chem.* **76**, 296.
Scott, R. L. 1973 Third International Conference on Chemical Thermodynamics (Baden, Austria): preprints, vol. II, p. 220.

PHILOSOPHICAL TRANSACTIONS OF THE ROYAL SOCIETY A MATHEMATICAL, PHYSICAL & ENGINEERING SCIENCES

Scott, R. L. 1977 *J. chem. Soc. Faraday Trans.* II **73**, 356.
Scott, R. L. & van Konynenburg, P. H. 1970 *Discuss. Faraday Soc.* **49**, 87.
van Konynenburg, P. H. 1968 Dissertation, University of California, Los Angeles.
van Laar, J. J. 1904–05 *Proc. Sect. Sci. K. ned. Akad. Wet.* **7**, 517, 636, 646.
van Laar, J. J. 1905 *Proc. Sect. Sci. K. ned. Akad. Wet.* **8**, 33.
van Laar, J. J. 1906 *Proc. Sect. Sci. K. ned. Akad. Wet.* **9**, 226.
van Laar, J. J. 1910 *Z. phys. Chem.* **72**, 723.
van der Waals, J. D. 1890 *Z. phys. Chem.* **5**, 133.
van der Waals, J. D. 1899 *Die Kontinuität des gasförmigen und flüssigen Zustandes.* I. Single component systems (2nd edn). Leipzig: Barth.
van der Waals, J. D. 1900 *Die Kontinuität des gasförmigen und flüssigen Zustandes.* II. Binary mixtures. Leipzig: Barth.
van der Waals, J. D. 1906–07 *Proc. Sect. Sci. K. ned. Akad. Wet.* **9**, 621, 727, 826.
van der Waals, J. D. 1907–08 *Proc. Sect. Sci. K. ned. Akad. Wet.* **10**, 56, 123, 183.
van der Waals, J. D. 1908–09 *Proc. Sect. Sci. K. ned. Akad. Wet.* **11**, 146, 187, 201, 317, 426, 477, 698, 816, 890.
van der Waals, J. D. 1911–12 *Proc. Sect. Sci. K. ned. Akad. Wet.* **14**, 504, 655, 875, 1049, 1217.
van der Waals, J. D. 1912–13 *Proc. Sect. Sci. K. ned. Akad. Wet.* **15**, 602.
Widom, B. 1973 *J. phys. Chem.* **77**, 2196.

PHILOSOPHICAL TRANSACTIONS OF THE ROYAL SOCIETY A MATHEMATICAL, PHYSICAL & ENGINEERING SCIENCES